

Design and Analysis of a Concatenated Code for Intersymbol Interference Wiretap Channels

Aria Nouri¹, Graduate Student Member, IEEE, Reza Asvadi¹, Senior Member, IEEE, and Jun Chen¹, Senior Member, IEEE

Abstract—We propose a two-stage concatenated coding scheme for reliable and information-theoretically secure communication over intersymbol interference wiretap channels. Motivated by the theoretical coding strategies that achieve the secrecy capacity, our scheme integrates low-density parity-check (LDPC) codes in the outer stage, forming a nested structure of wiretap codes, with trellis codes in the inner stage to improve achievable secure rates. The trellis code is specifically designed to transform the uniformly distributed codewords produced by the LDPC code stage into a Markov process, achieving tight lower bounds on the secrecy capacity. We further estimate the information leakage rate of the proposed coding scheme using an upper bound. To meet the weak secrecy criterion, we optimize degree distributions of the irregular LDPC codes at the outer stage, essentially driving the estimated upper bound on the information leakage rate to zero.

Index Terms—Intersymbol interference (ISI), wiretap channel, physical-layer security, superchannel, concatenated codes, density evolution, low-density parity-check (LDPC) codes, trellis codes.

I. INTRODUCTION

A. Motivation

Classical cryptography addresses secrecy requirements by assuming that eavesdroppers have limited computational capabilities. This assumption prevents eavesdroppers from solving computationally complex problems, thereby safeguarding the cryptosystems from cryptanalysis. While breaking a robust cryptosystem in a reasonable time is currently infeasible, the evolution of prospective quantum computers poses a threat to the security of existing cryptographic protocols [2]. Moreover, the absence of security at the physical layer allows eavesdroppers to intercept and store the encrypted data, potentially breaking the encryption once the promised computational capabilities catch up. Alternatively, quantum cryptography aims to leverage the postulates of quantum mechanics to achieve loophole-free unconditional security [3]. Though this field of research has brought revolutionary directions in near-future communication systems [4], the proposed network protocol stack faces challenges in compatibility with existing infrastructures [5] and requires additional assumptions to achieve the promised unconditional security [6].

Information-theoretic physical-layer security [7], [8] properly overcomes the mentioned drawbacks: (i) by employing

secrecy measures that are independent of the computational capability of eavesdroppers, security is assured even against adversaries with unlimited computational power; (ii) by operating at the physical layer of the existing infrastructure, it ensures that intercepting and analyzing the eavesdropper’s observations do not yield additional information about the secret data. Despite these advantages, since a majority of information-theoretic proofs are developed within idealized channel conditions, it is mostly infeasible to apply these results for securing non-ideal practical communication systems because the criteria for ensuring information-theoretic security need to be fulfilled rigorously and measured explicitly [9].¹

Frequency selectivity is a non-ideal phenomenon that causes intersymbol interference (ISI), degrading the performance of wireless communication systems ranging from narrow-band [10] to ultra-wideband [11]. In phased array antennas that are pivotal for millimeter-wave communication systems—due to their ability to support high-frequency bands, enabling the multi-gigabit-per-second data rates and low latency required by 5G and beyond networks—ISI arises from time delays across different antenna elements in both transmitted and received signals [12]. The existing equalization techniques are effective only when the delay exceeds a small fraction of the symbol interval, imposing several limitations on (i) the number of array elements, (ii) the scan angle,² and (iii) the symbol rate of the communication system (see Appendix A). In this paper, we focus on a practical scenario with full ISI, i.e., the delay significantly exceeds the symbol interval. We address the coding problem of achieving reliable and information-theoretically secure communication in an ISI wiretap channel (ISI-WTC) setup [13], where the transmitter (Alice) is connected to a legitimate receiver (Bob, labeled by “B”) and to an eavesdropper (Eve, labeled by “E”) by two independent ISI channels.

B. Background and Related Works

Designing practical methods for reliable transmission over point-to-point ISI channels is a well-established research topic

¹Aria Nouri and Reza Asvadi are with the Department of Telecommunications, Faculty of Electrical Engineering, Shahid Beheshti University, Tehran 1983963113, Iran (e-mails: ariya@iee.org; r_asvadi@sbu.ac.ir).

²Jun Chen is with the Department of Electrical and Computer Engineering, McMaster University, Hamilton, ON L8S 4K1, Canada (e-mail: chenjun@mcmaster.ca).

This paper was presented in part at the IEEE International Symposium on Information Theory (ISIT), Espoo, Finland, in June 2022 [1].

¹A limited amount of error caused by ignoring the non-ideal properties of practical communication channels is tolerable when measuring the *reliability* of the communication. However, ignoring these non-ideal properties when measuring the *secrecy* performance might lead to unintended leakage of private information, which is unacceptable.

²The scan angle refers to the maximum angular range over which the antenna array can steer its main beam, typically measured from the array’s boresight (central axis) to the extreme angles in both directions.

in the literature of coding and signal processing societies [14]–[23]. For brevity, we only review a particular class of turbo-based error correction schemes [24] related to this work.

The incorporation of maximum *a posteriori* symbol detectors [25]–[27] with linear block codes has led to the development of soft-estimation decoding architectures over ISI channels, commonly referred to as turbo-equalizers [16]–[21]. Kavčić *et al.* [20] extended the density evolution method [28] to analyze the asymptotic performance of low-density parity-check (LDPC) codes within the turbo-equalizer framework. Varnica and Kavčić [29] further demonstrated that the information rate achieved by an independent and uniformly distributed (i.u.d.) input process can be closely approached using suitably optimized LDPC codes within the turbo-equalizer structure. More recently, it has been shown in [30] and [31] that the complexity of turbo-equalizers can be reduced by solving the optimization-based decoding problem [32] with the approach presented in [33].

Soriaga *et al.* [34] addressed the design of a multilevel coding scheme paired with a multistage decoding algorithm for ISI channels. The decoder proposed in [34] operates without requiring interaction between all stages during each iteration and approaches the i.u.d. information rate as the number of decoding stages increases. To the best of our knowledge, the only coding scheme that surpasses the i.u.d. information rate and approaches the capacity of general point-to-point ISI channels is the one proposed in [35], commonly referred to as matched information rate codes. Specifically, this code is a two-stage concatenated coding scheme comprising an inner-stage trellis code and an outer-stage LDPC code.

Coding for secrecy over Gaussian wiretap channels [36] has received considerable attention over the past decade [37]–[42]. However, despite the practical importance of ensuring security in channels with memory [13], [43], [44], the design of codes for secure transmission over such channels remains a challenge. To the best of our knowledge, this work is the first to specifically tackle code design for Gaussian wiretap channels with ISI. By leveraging optimized Markov sources over ISI-WTCs [13] and extending the design principles established in [35], we introduce a concatenated coding scheme for ISI-WTCs, meeting both reliability and secrecy constraints.

C. Contributions and Organization

In the following, we outline the main contributions of this work.

- We show that ISI-WTCs are equivalent to the stationary wiretap channels considered in [45] when employing vector inputs and vector outputs; thus, we derive the secrecy capacity of ISI-WTCs by leveraging the results from [45]. Drawing on insights from the theoretical coding strategies that achieve the secrecy capacity, we utilize a trellis code at the inner stage, enabling our coding scheme to approach a numerical lower bound on the secrecy capacity, known as the constrained secrecy capacity [13]. We further show that the inner-stage trellis code effectively shapes the spectrum of the transmitted codewords, concentrating most of the available power in

frequency ranges where Bob’s channel has a higher gain-to-noise power spectrum ratio than Eve’s channel, thereby achieving positive secure rates even when Eve’s channel has a higher point-to-point capacity than Bob’s channel.

- We implement the nested structure of wiretap codes [46] using punctured LDPC codes at the outer stage. To evaluate the secrecy performance, we estimate a numerical upper bound on the rate of information leakage achieved by the proposed code over ISI-WTCs. Subsequently, for a fixed secure rate, we optimize degree distributions of the outer LDPC code stage to reduce the estimated upper bound essentially to zero, thereby satisfying the weak secrecy criterion [8]. Additionally, we extend the density evolution method from [20] to analyze the asymptotic performance of the proposed two-stage code and optimize degree distributions of the LDPC codes at the outer stage.
- In the asymptotic regime, the proposed code satisfies the reliability and the weak secrecy criteria at secure rates within 0.42 dB of the constrained secrecy capacity. In the finite blocklength regime, with a blocklength of 10^5 , the code achieves a bit-error rate of 10^{-5} at Bob’s decoder and meets the weak secrecy criterion while remaining within 3.6dB of the constrained secrecy capacity.

The remainder of this paper is organized as follows. Section II introduces the channel model and key preliminary concepts. Section III establishes the secrecy capacity of ISI-WTCs and illuminates the connection between secrecy capacity-achieving codes and the proposed two-stage coding scheme. Section IV introduces the factor graph of the two-stage concatenated code and generalizes the density evolution method. Section V describes the code design procedure. Section VI presents the performance of the proposed code in the finite blocklength regime. Finally, Section VII concludes the paper.

D. Notation

The sets of integers, reals, and complex numbers are denoted by \mathbb{Z} , \mathbb{R} , and \mathbb{C} , respectively. Also, a ring of polynomials over \mathbb{C} with the indeterminate D is denoted by $\mathbb{C}[D]$. Other than that, sets are denoted by calligraphic letters, e.g., \mathcal{S} . The Cartesian product of two sets \mathcal{X} and \mathcal{Y} is written as $\mathcal{X} \times \mathcal{Y}$, and the n -fold Cartesian product of \mathcal{X} with itself is written as \mathcal{X}^n . If \mathcal{X} is a finite set, then its cardinality is denoted by $|\mathcal{X}|$. Moreover, for a finite vector space \mathcal{V} , its dimension is represented by $\dim(\mathcal{V})$.

Random variables are denoted by upper-case italic letters, e.g., X , their realizations by the corresponding lower-case letters, e.g., x , and the set of possible values by the corresponding calligraphic letters, e.g., \mathcal{X} . Random vectors are denoted by upper-case boldface italic letters, e.g., \mathbf{X} , and their realizations by the corresponding lower-case letters, e.g., \mathbf{x} . For a positive value of $n \in \mathbb{Z}$, a time-indexed ($t \in \mathbb{Z}$) vector of random variables is denoted by $\mathbf{X}^n(t) \triangleq (X(n(t-1)+1), \dots, X(nt))$, and its realization is denoted by $\mathbf{x}^n(t) \triangleq (x(n(t-1)+1), \dots, x(nt))$. The time index t is dropped from the vectors starting with $t = 1$, e.g., \mathbf{X}^n is used instead of $\mathbf{X}^n(1)$. The convolution of two vectors \mathbf{x} and \mathbf{y} is denoted by $\mathbf{x} * \mathbf{y}$, and the n -time convolution of \mathbf{x} with itself

is denoted by $\mathbf{x}^{(*n)}$. Matrices and higher-dimensional arrays are denoted by upper-case boldface letters, e.g., \mathbf{H} .

The probability of an event ξ is represented by $\Pr(\xi)$. Additionally, $p_X(\cdot)$ denotes the probability mass function (PMF) of a discrete random variable X , and $p_{Y|X}(\cdot|x)$ represents the conditional PMF of a discrete random variable Y given $X = x$. A similar notation is used for probability density functions (PDFs) when dealing with continuous random variables. The entropy of a random variable X and the mutual information between two random variables X and Y are denoted by $H(X)$ and $I(X; Y)$, respectively. The Kullback–Leibler (KL) divergence between two PMFs $p_X(\cdot)$ and $p_Y(\cdot)$ over the same finite alphabet \mathcal{X} is defined as

$$D_{\text{KL}}(p_X || p_Y) \triangleq \sum_{x \in \mathcal{X}} p_X(x) \log \frac{p_X(x)}{p_Y(x)}.$$

In addition, the independence between two random variables X and Y is denoted by $X \perp Y$.

For $x \in \mathbb{R}$, the expression $(x)^+$ stands for $\max\{x, 0\}$. Similarly, for a real-valued function $f(\cdot)$, the expression $f^+(\cdot)$ is used to represent $(f(\cdot))^+$. Lastly, $\delta(\cdot)$ refers to the Kronecker delta function, and $\mathbf{1}(\cdot)$ represents the indicator function.

II. PRELIMINARIES AND DEFINITIONS

In this section, we present finite-state models for inter-symbol interference (ISI) channels, ISI wiretap channels (ISI-WTCs), and their corresponding trellis representations. We then define trellis codes and introduce a joint finite-state model for trellis codes applied at the input of the ISI-WTCs.

A. Channel Models

An ISI channel is characterized by a transfer polynomial $g[D] \triangleq \sum_{r=0}^{\nu} g(r) \cdot D^r \in \mathbb{C}[D]$, where $\nu \in \mathbb{Z}$ is referred to as the memory length. This channel has an input process $\{X(t)\}_{t \in \mathbb{Z}}$, a noiseless output process $\{U(t)\}_{t \in \mathbb{Z}}$ with $U(t) \triangleq \sum_{r=0}^{\nu} g(r) \cdot X(t-r)$, and a noisy output process $\{Y(t)\}_{t \in \mathbb{Z}}$ with $Y(t) \triangleq U(t) + W(t)$, where $W(t) \in \mathbb{C}$ is a circularly-symmetric complex Gaussian random variable with mean zero, variance per dimension σ^2 , and $W(t) \perp X(t)$, and where $X(t), U(t), Y(t) \in \mathbb{C}$, for all $t \in \mathbb{Z}$. Clearly, any ISI channel is parameterized by a pair $(g[D], \sigma^2) \in \mathbb{C}[D] \times \mathbb{R}$.

In this paper, we only consider ISI channels having $\mathcal{X} \subsetneq \mathbb{C}$ and $\nu < \infty$. These channels are a particular case from a more general class of channels defined as follows.

Definition 1 (Finite-State Machine Channel (FSMC)). A time-invariant FSMC consists of an input process $\{X(t)\}_{t \in \mathbb{Z}}$, an output process $\{Y(t)\}_{t \in \mathbb{Z}}$, and a state process $\{S_f(t)\}_{t \in \mathbb{Z}}$, where $X(t) \in \mathcal{X}$, $Y(t) \in \mathcal{Y}$, and $S_f(t) \in \mathcal{S}_f$, for all $t \in \mathbb{Z}$, and \mathcal{S}_f and \mathcal{X} are assumed to be finite. Let $B_f(t) \triangleq (S_f(t-1), X(t), S_f(t))$, referred to as a branch, and let \mathcal{B}_f denote the set of all triples $b_f(t) = (s_f(t-1), x(t), s_f(t))$ where $p_{B_f(t)}(b_f(t))$ is allowed to be nonzero.³ For any positive

integer N , the joint PMF/PDF of \mathbf{B}_f^N and \mathbf{Y}^N conditioned on $S_f(0) = s_f(0)$ and $\mathbf{X}^N = \mathbf{x}^N$ is

$$\begin{aligned} & p_{\mathbf{B}_f^N, \mathbf{Y}^N | S_f(0), \mathbf{X}^N}(\mathbf{b}_f^N, \mathbf{y}^N | s_f(0), \mathbf{x}^N) \\ &= \prod_{t=1}^N p_{B_f(t), Y(t) | S_f(t-1), X(t)}(b_f(t), y(t) | s_f(t-1), x(t)), \end{aligned} \quad (1)$$

where the factor on the right-hand side (RHS) is independent of t . \square

Remark 1. As mentioned at the beginning of this section, an ISI channel described by the pair $(g[D] \triangleq \sum_{t=0}^{\nu} g(t) \cdot D^t, \sigma^2)$, having a finite memory $\nu < \infty$ and a finite input alphabet $\mathcal{X} \subsetneq \mathbb{C}$, is a special case of the FSMC. Specifically, let $s_f(t) \triangleq \mathbf{x}^{\nu}(\frac{t}{\nu})$ with $\mathcal{S}_f \triangleq \mathcal{X}^{\nu}$, which establishes a one-to-one correspondence between $(s_f(t-1), x(t))$ and $(s_f(t-1), b_f(t))$, for all $t \in \mathbb{Z}$. Then, the factor on the RHS of (1) becomes

$$\begin{aligned} & p_{B_f(t), Y(t) | S_f(t-1), X(t)}(b_f(t), y(t) | s_f(t-1), x(t)) \\ &= p_{B_f(t) | S_f(t-1), X(t)}(b_f(t) | s_f(t-1), x(t)) \\ & \quad \cdot p_{Y(t) | S_f(t-1), X(t)}(y(t) | s_f(t-1), x(t)), \end{aligned}$$

in which $p_{B_f(t) | S_f(t-1), X(t)}(b_f(t) | s_f(t-1), x(t)) \triangleq \mathbf{1}(b_f(t) = (s_f(t-1), x(t), s_f(t)))$, and

$$\begin{aligned} & p_{Y(t) | S_f(t-1), X(t)}(y(t) | s_f(t-1), x(t)) \\ & \triangleq \frac{1}{2\pi\sigma^2} \cdot \exp\left(-\frac{|y(t) - u(t)|^2}{2\sigma^2}\right), \end{aligned} \quad (2)$$

where $u(t) \triangleq \sum_{r=0}^{\nu} g(r) \cdot x(t-r)$. \square

Definition 2 (Trellis Diagram). A trellis diagram is a two-dimensional directed graph, visualizing the state alphabet of a finite-state machine by ordered nodes grouped in consecutive vertical partitions, with each partition corresponding to a time index. The time evolution of the states is represented by branches connecting nodes in successive partitions. Since all finite-state machines considered in this work are time-invariant and the state processes have a memory order of one, a single trellis section comprising two successive partitions is sufficient to demonstrate all valid state transitions. For notational convenience, realizations of the starting and the ending states in the trellis sections are denoted by $i, j \in \mathbb{Z}$, respectively. \square

According to $s_f(t) \triangleq \mathbf{x}^{\nu}(\frac{t}{\nu})$ and $|\mathcal{S}_f| \triangleq |\mathcal{X}|^{\nu}$ in Remark 1, parallel branches do not appear in the trellis section of the FSMCs used to model the ISI channels. Therefore, each branch $(i, x(t), j) \in \mathcal{B}_f$ of the FSMC is uniquely specified by the pair $(i, j) \in \mathcal{S}_f^2$. Let $\check{\mathcal{B}}_f$ be a set of all pairs $(i, j) \in \mathcal{S}_f^2$ where $(i, x(t), j) \in \mathcal{B}_f$. Since one can define a bijective map between \mathcal{B}_f and $\check{\mathcal{B}}_f$, we use $\check{\mathcal{B}}_f \subseteq \mathcal{S}_f^2$ as a simplified alternative instead of the branch alphabet \mathcal{B}_f . Accordingly, we associate a label $\beta_f(i, j) \triangleq (i, x, u, j)$ to $b_f(t) = (i, x(t), j)$, for all $b_f(t) \in \mathcal{B}_f$, where $x \in \mathcal{X}$ is the input compatible with the realization of the branch $(i, j) \in \check{\mathcal{B}}_f$ (equivalently $(i, x, j) \in \mathcal{B}_f$) and $u \in \mathbb{C}$ is the associated noiseless output. We sketch the trellis

³Due to the similarity in notations used for various finite-state machines, we distinguish random variables and alphabet sets corresponding to states and branches of each finite-state machine using specific subscripts.

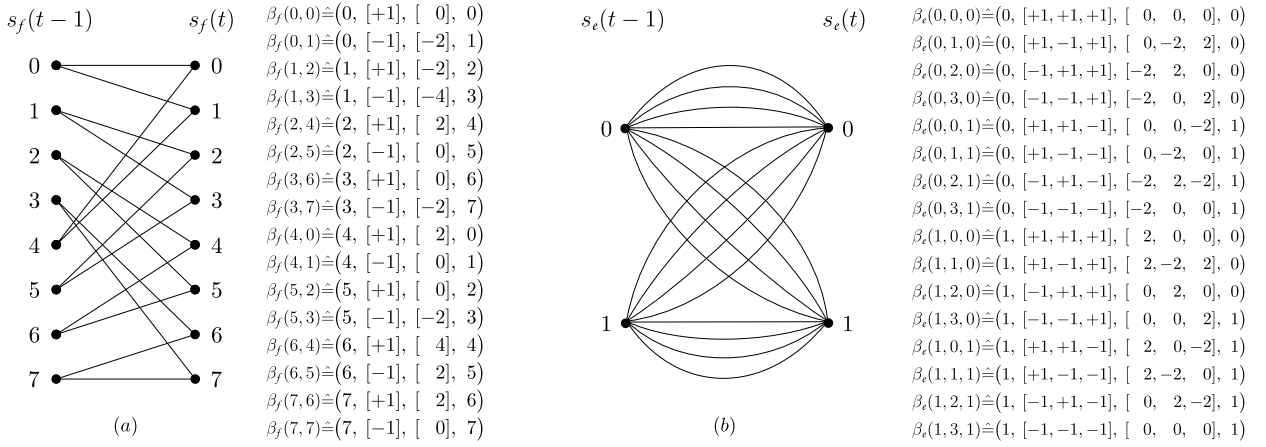


Fig. 1: (a) Trellis section of an FSMC, representing the EPR4 channel and the collection of branches $\beta_f(i, j) = (i, x, u, j)$ for all $(i, j) \in \tilde{\mathcal{B}}_f$. (b) Trellis section of a 3-rd order E-FSMC, representing the DICODE channel and the collection of branches $\beta_e(i, \ell, j) \triangleq (i, \mathbf{x}^3, \mathbf{u}^3, j)$ for all $(i, \ell, j) \in \tilde{\mathcal{B}}_e$.

section of an FSMC, representing an EPR4 channel⁴ with the (unnormalized) transfer polynomial $g[D] = 1 + D - D^2 - D^3$ and the input alphabet $\mathcal{X} \triangleq \{-1, +1\}$ in Fig. 1(a).

The following definition introduces an auxiliary model, extending Definition 1, and provides the parameters required for designing the inner trellis code stage in Section V-A.

Definition 3 (Extended FSMC (E-FSMC)). An E-FSMC of order $n \in \mathbb{Z}$ is a time-invariant finite-state machine, comprising n consecutive identical FSMCs as in Definition 1. Indeed, the E-FSMC has an input process $\{\mathbf{X}^n(t)\}_{t \in \mathbb{Z}}$, an output process $\{\mathbf{Y}^n(t)\}_{t \in \mathbb{Z}}$, and a state process $\{S_e(t)\}_{t \in \mathbb{Z}}$, where $X(t) \in \mathcal{X}$, $Y(t) \in \mathcal{Y}$, and $S_e(t) \in \mathcal{S}_e$, for all $t \in \mathbb{Z}$, and \mathcal{S}_e and \mathcal{X} are assumed to be finite. Let $B_e(t) \triangleq (S_e(t-1), \mathbf{X}^n(t), S_e(t))$ and let \mathcal{B}_e be a set of all triples $b_e(t) = (s_e(t-1), \mathbf{x}^n(t), s_e(t))$ where $p_{B_e(t)}(b_e(t))$ is allowed to be nonzero. Each realization of the branch $b_e(t) \in \mathcal{B}_e$ at the n -th order E-FSMC coincides with realizing n legal consecutive branches⁵ at the corresponding FSMC, i.e., $(s_e(t-1), b_e(t)) \triangleq (s_f(n(t-1)), \mathbf{b}_f^n(t))$. Hence, the PMF of $B_e(t)$ conditioned on $S_e(t-1) = s_e(t-1)$ becomes

$$\begin{aligned} p_{B_e(t)|S_e(t-1)}(b_e(t)|s_e(t-1)) &\triangleq p_{\mathbf{B}_f^n(t)|S_f(n(t-1))}(\mathbf{b}_f^n(t)|s_f(n(t-1))) \\ &= \prod_{l=n(t-1)+1}^{nt} p_{B_f(l)|S_f(l-1)}(b_f(l)|s_f(l-1)). \end{aligned}$$

For any positive integer N , the joint PMF/PDF of \mathbf{B}_e^N and \mathbf{Y}^{nN} conditioned on $S_e(0) = s_e(0)$ and $\mathbf{X}^{nN} = \mathbf{x}^{nN}$ is

$$p_{\mathbf{B}_e^N, \mathbf{Y}^{nN}|S_e(0), \mathbf{X}^{nN}}(\mathbf{b}_e^N, \mathbf{y}^{nN}|s_e(0), \mathbf{x}^{nN})$$

⁴In this section, unnormalized magnetic recording channels are used as simplified models to introduce the general concept of the trellises. While these channels may have limited applications in wiretapping scenarios, the same trellises will be employed in later sections to model received signals from phased arrays in 5G base stations (Appendix A).

⁵Legal consecutive realizations of branches are branch sequences where the ending state of each branch equals the starting state of the next. All other sequences are considered illegal.

$$= \prod_{t=1}^N p_{B_e(t), \mathbf{Y}^n(t)|S_e(t-1), \mathbf{X}^n(t)}(b_e(t), \mathbf{y}^n(t)|s_e(t-1), \mathbf{x}^n(t)), \quad (3)$$

where the factor on the RHS is independent of t . \square

Remark 2. In the case of ISI channels, the factor on the RHS of (3) becomes

$$\begin{aligned} &p_{B_e(t), \mathbf{Y}^n(t)|S_e(t-1), \mathbf{X}^n(t)}(b_e(t), \mathbf{y}^n(t)|s_e(t-1), \mathbf{x}^n(t)) \\ &= p_{B_e(t)|S_e(t-1), \mathbf{X}^n(t)}(b_e(t)|s_e(t-1), \mathbf{x}^n(t)) \\ &\quad \cdot p_{\mathbf{Y}^n(t)|S_e(t-1), \mathbf{X}^n(t)}(\mathbf{y}^n(t)|s_e(t-1), \mathbf{x}^n(t)), \end{aligned}$$

in which $p_{B_e(t)|S_e(t-1), \mathbf{X}^n(t)}(b_e(t)|s_e(t-1), \mathbf{x}^n(t)) \triangleq \mathbb{1}(b_e(t) = (s_e(t-1), \mathbf{x}^n(t), s_e(t)))$, and

$$\begin{aligned} &p_{\mathbf{Y}^n(t)|S_e(t-1), \mathbf{X}^n(t)}(\mathbf{y}^n(t)|s_e(t-1), \mathbf{x}^n(t)) \\ &\triangleq \prod_{l=(t-1)n+1}^{nt} p_{Y(l)|S_f(l-1), X(l)}(y(l)|s_f(l-1), x(l)) \\ &= \frac{1}{(2\pi\sigma^2)^n} \cdot \exp\left(-\sum_{l=(t-1)n+1}^{nt} \frac{|y(l) - u(l)|^2}{2\sigma^2}\right), \end{aligned}$$

where the last equality follows from (2). \square

A set of all possible state transitions of the E-FSMC is also visualized by a single trellis section as in Definition 2. Let $L_e(i, j) \in \mathbb{Z}$ be the number of parallel branches between the pair of states $(i, j) \in \mathcal{S}_e^2$. Then, each branch $(i, \mathbf{x}^n, j) \in \mathcal{B}_e$ of the E-FSMC is uniquely specified by the triple (i, ℓ, j) , where $0 \leq \ell \leq L_e(i, j) - 1$ identifies $L_e(i, j)$ distinct branches between $(i, j) \in \mathcal{S}_e^2$. Let $\tilde{\mathcal{B}}_e$ be a set of triples (i, ℓ, j) , specifying all valid branches $(i, \mathbf{x}^n, j) \in \mathcal{B}_e$. Since one can define a bijective map between \mathcal{B}_e and $\tilde{\mathcal{B}}_e$, we use $\tilde{\mathcal{B}}_e$ as a simplified alternative instead of the branch alphabet \mathcal{B}_e . Accordingly, we associate a label $\beta_e(i, \ell, j) \triangleq (i, \mathbf{x}^n, \mathbf{u}^n, j)$ to $b_e(t) = (i, \mathbf{x}^n(t), j)$, for all $b_e(t) \in \mathcal{B}_e$, where $0 \leq \ell \leq L_e(i, j) - 1$, $\mathbf{x}^n \in \mathcal{X}^n$ is the n -tuple input compatible with the realization of the branch $(i, \ell, j) \in \tilde{\mathcal{B}}_e$ (equivalently $(i, \mathbf{x}^n, j) \in \mathcal{B}_e$), and $\mathbf{u}^n \in \mathcal{C}^n$ is the associated noiseless n -tuple output. We sketch the trellis section of a third-order E-FSMC, representing a

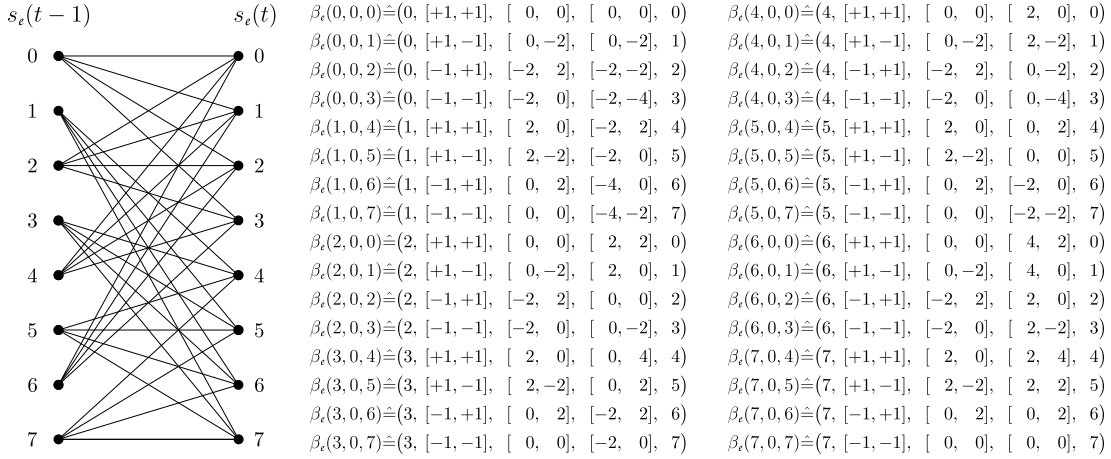


Fig. 2: Trellis section of a 2-nd order E-FSMC that represents an ISI-WTC, comprising a DICODE channel as Bob's channel and an EPR4 channel as Eve's channel. Each branch of the trellis section is labeled by $\beta_c(i, \ell, j) \triangleq (i, \mathbf{x}^2, \mathbf{u}^2, \mathbf{v}^2, j)$ for all $(i, \ell, j) \in \tilde{\mathcal{B}}_c$.

DICODE channel with the (unnormalized) transfer polynomial $g[D] = 1 - D$ and the input alphabet $\mathcal{X} \triangleq \{-1, +1\}$ in Fig. 1(b).

Definition 4 (Intersymbol Interference Wiretap Channel (ISI-WTC)). An ISI-WTC is a wiretap channel where Alice transmits data symbols over Bob's channel and over Eve's channel, which are both assumed to be ISI channels. Specifically, Bob's channel is described by $(g_B[D], \sigma_B^2)$ with the transfer polynomial $g_B[D] = \sum_{r=0}^{\nu_B} g_B(r) \cdot D^r$, a noiseless output process $\{U(t)\}_{t \in \mathbb{Z}}$, a noise process $\{W_B(t)\}_{t \in \mathbb{Z}}$, and a noisy output process $\{Y(t)\}_{t \in \mathbb{Z}}$. Similarly, Eve's channel is described by $(g_E[D], \sigma_E^2)$ with the transfer polynomial $g_E[D] = \sum_{r=0}^{\nu_E} g_E(r) \cdot D^r$, a noiseless output process $\{V(t)\}_{t \in \mathbb{Z}}$, a noise process $\{W_E(t)\}_{t \in \mathbb{Z}}$, and a noisy output process $\{Z(t)\}_{t \in \mathbb{Z}}$. The random variables $W_B(t)$ and $W_E(t)$ are independent from each other and independent from the input process for all $t \in \mathbb{Z}$. Clearly, the entire ISI-WTC is parameterized by a quadruple $(g_B[D], g_E[D], \sigma_B^2, \sigma_E^2)$. \square

Notice that the FSMCs, the E-FSMCs, and their associated trellises are also utilized to represent ISI-WTCs. Since Bob's channel is assumed to be independent of Eve's channel, these generalizations are straightforward. We illustrate this using the following example. Consider an ISI-WTC with an input alphabet $\mathcal{X} \triangleq \{-1, +1\}$, where Bob's channel is a DICODE channel and Eve's channel is an EPR4 channel. The trellis section of the second-order E-FSMC, corresponding to this ISI-WTC is depicted in Fig. 2. Each branch of the trellis section is labeled by $\beta_c(i, \ell, j) \triangleq (i, \mathbf{x}^2, \mathbf{u}^2, \mathbf{v}^2, j)$, where $\mathbf{x}^2 \in \{-1, +1\}^2$ is the input compatible with the realization of the branch $(i, \ell, j) \in \tilde{\mathcal{B}}_c$ (equivalently $(i, \mathbf{x}^2, j) \in \mathcal{B}_c$), and $\mathbf{u}^2, \mathbf{v}^2 \in \mathbb{R}^2$ are, respectively, the associated noiseless outputs of Bob's and Eve's channels.

B. Trellis Codes and Superchannel

The trellis representation of error correction codes offers an effective framework for analyzing the statistical properties of codewords generated by a coding scheme without taking the algebraic structure of the code into account [47].

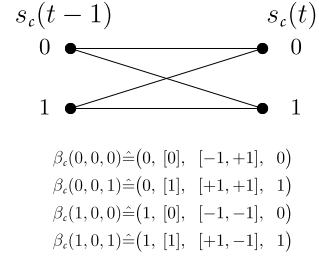


Fig. 3: Wolf-Ungerboeck code of rate 1/2 and the collection of branches $\beta_c(i, \ell, j) = (i, d, \mathbf{x}^2, j)$ for all $(i, \ell, j) \in \tilde{\mathcal{B}}_c$.

Definition 5 (Trellis Code). Without loss of generality, any channel code that can be represented by a time-invariant finite-state machine is referred to as a trellis code in this paper. Specifically, a trellis code of rate m/n (with $m \in \mathbb{Z}$, $n \in \mathbb{Z}$) is a time-invariant finite-state machine comprising an input process $\{\mathbf{D}^m(t)\}_{t \in \mathbb{Z}}$, an output process $\{\mathbf{X}^n(t)\}_{t \in \mathbb{Z}}$, and a state process $\{S_c(t)\}_{t \in \mathbb{Z}}$, where $D(t) \in \{0, 1\}$, $X(t) \in \mathcal{X}$, $S_c(t) \in \mathcal{S}_c$, for all $t \in \mathbb{Z}$, \mathcal{S}_c and \mathcal{X} are assumed to be finite, and $m \leq n \cdot \log |\mathcal{X}|$. Let $B_c(t) \triangleq (S_c(t-1), \mathbf{D}^m(t), S_c(t))$ and let \mathcal{B}_c be a set of all triples $b_c(t) = (s_c(t-1), \mathbf{d}^m(t), s_c(t))$ where $p_{B_c(t)}(b_c(t))$ is allowed to be nonzero. For a binary trellis code of rate m/n , each realization of the branch $b_c(t) \in \mathcal{B}_c$ maps an m -bit input message $\mathbf{d}^m(t) \in \{0, 1\}^m$ to an n -symbol output codeword $\mathbf{x}^n(t) \in \{-1, +1\}^n$, at time $t \in \mathbb{Z}$. Thus, there are totally 2^m branches $b_c(t) \in \mathcal{B}_c$ emanating from each state $s_c(t-1) \in \mathcal{S}_c$ of the trellis code (one branch for each binary input of length m). \square

Due to the time-invariance assumption, a single trellis section is sufficient to demonstrate all valid branches between the successive states of the trellis code. Let $L_c(i, j) \in \mathbb{Z}$ be the number of parallel branches between the pair of states $(i, j) \in \mathcal{S}_c^2$. Then, each branch $(i, \mathbf{d}^m(t), j) \in \mathcal{B}_c$ of the trellis code is uniquely specified by a triple (i, ℓ, j) , where $0 \leq \ell \leq L_c(i, j) - 1$ identifies $L_c(i, j)$ distinct branches between $(i, j) \in \mathcal{S}_c^2$. Let $\tilde{\mathcal{B}}_c$ be a set of triples (i, ℓ, j) , specifying all valid branches $(i, \mathbf{d}^m(t), j)$ in \mathcal{B}_c . Since one can define a bijective map between \mathcal{B}_c and $\tilde{\mathcal{B}}_c$, we use $\tilde{\mathcal{B}}_c$ as a simplified alternative instead of the branch alphabet \mathcal{B}_c .

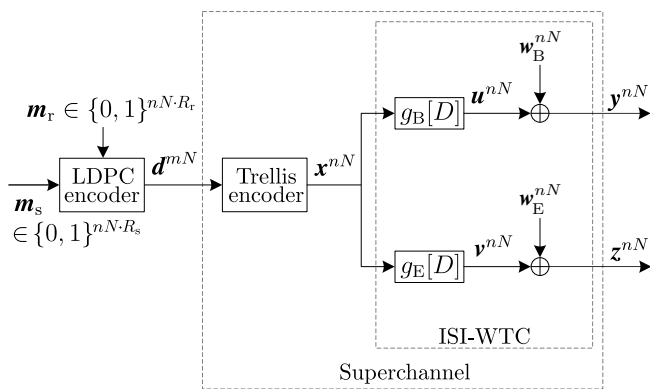


Fig. 4: Block diagram of the proposed concatenated coding scheme, the ISI-WTC, and the corresponding superchannel. Note that the trellis code under consideration has a rate of m/n .

Accordingly, we associate a label $\beta_c(i, \ell, j) \triangleq (i, \mathbf{d}^m, \mathbf{x}^n, j)$ to $b_c(t) = (i, \mathbf{d}^m(t), j)$, for all $b_c(t) \in \mathcal{B}_c$, where $0 \leq \ell \leq L_c(i, j) - 1$, $\mathbf{d}^m \in \{0, 1\}^m$ is the m -tuple input message compatible with the realization of the branch $(i, \ell, j) \in \tilde{\mathcal{B}}_c$ (equivalently $(i, \mathbf{d}^m, j) \in \mathcal{B}_c$), and $\mathbf{x}^n \in \{-1, +1\}^n$ is the associated n -tuple output codeword. As an example, the trellis representation of the Wolf-Ungerboeck code [48] of rate $1/2$ is depicted in Fig. 3.

Definition 6 (Superchannel). A superchannel is a time-invariant finite-state machine, modeling the concatenation of a binary trellis code of rate m/n (Definition 5), and an n -th order E-FSMC (Definition 3) representing an ISI-WTC (see Fig. 4). The superchannel comprises an input process $\{\mathbf{D}^m(t)\}_{t \in \mathbb{Z}}$ corresponding to the input messages of the trellis code, an output process $\{\mathbf{Y}^n(t)\}_{t \in \mathbb{Z}}$ corresponding to Bob's observations, an output process $\{\mathbf{Z}^n(t)\}_{t \in \mathbb{Z}}$ corresponding to Eve's observations, and a state process $\{S(t)\}_{t \in \mathbb{Z}}$. Indeed, $D(t) \in \{0, 1\}$, $Y(t), Z(t) \in \mathbb{C}$, and $S(t) \in \mathcal{S}$, for all $t \in \mathbb{Z}$, and \mathcal{S} is finite. Let $B(t) \triangleq (S(t-1), \mathbf{D}^m(t), S(t))$ and let \mathcal{B} be a set of all triples $b(t) = (s(t-1), \mathbf{d}^m(t), s(t))$ where $p_{B(t)}(b(t))$ is allowed to be nonzero. Each realization of an m -tuple input $\mathbf{d}^m(t) \in \{0, 1\}^m$ at time $t \in \mathbb{Z}$ coincides with realizing a branch $b(t) \in \mathcal{B}$ and emitting two n -tuple outputs: $\mathbf{y}^n(t) \in \mathbb{C}^n$ as Bob's observation and $\mathbf{z}^n(t) \in \mathbb{C}^n$ as Eve's observation. For any positive integer N , the joint PMF/PDF of $\mathbf{B}^N, \mathbf{Y}^{nN}, \mathbf{Z}^{nN}$ conditioned on $S(0) = s(0)$ and $\mathbf{D}^{mN} = \mathbf{d}^{mN}$ is

$$\begin{aligned} & p_{\mathbf{B}^N, \mathbf{Y}^{nN}, \mathbf{Z}^{nN} | S(0), \mathbf{D}^{mN}}(\mathbf{b}^N, \mathbf{y}^{nN}, \mathbf{z}^{nN} | s(0), \mathbf{d}^{mN}) \\ &= \prod_{t=1}^N p_{B(t) | S(t-1), \mathbf{D}^m(t)}(b(t) | s(t-1), \mathbf{d}^m(t)) \\ & \quad \cdot p_{\mathbf{Y}^n(t) | S(t-1), \mathbf{D}^m(t)}(\mathbf{y}^n(t) | s(t-1), \mathbf{d}^m(t)) \\ & \quad \cdot p_{\mathbf{Z}^n(t) | S(t-1), \mathbf{D}^m(t)}(\mathbf{z}^n(t) | s(t-1), \mathbf{d}^m(t)). \end{aligned}$$

This factorization is depicted as a normal factor graph [49] in Fig. 5. \square

Due to the time-invariance assumption, the finite-state machine modeling the superchannel is represented by a single trellis section as well. Let $L(i, j) \in \mathbb{Z}$ be the number of parallel branches between the pair of states $(i, j) \in \mathcal{S}^2$. Then, each branch $(i, \mathbf{d}^m(t), j) \in \mathcal{B}$ of the superchannel is uniquely specified by a triple (i, ℓ, j) , where $0 \leq \ell \leq L(i, j) - 1$

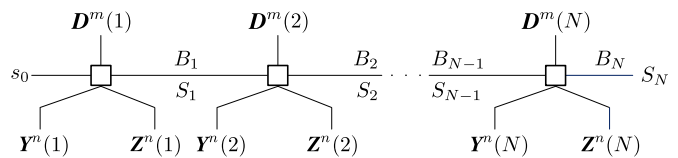


Fig. 5: Normal factor graph representation of the superchannel.

identifies $L(i, j)$ distinct branches between $(i, j) \in \mathcal{S}^2$. Let $\tilde{\mathcal{B}}$ be a set of triples (i, ℓ, j) , specifying all valid branches $(i, \mathbf{d}^m(t), j)$ in \mathcal{B} . Since one can define a bijective map between \mathcal{B} and $\tilde{\mathcal{B}}$, we use $\tilde{\mathcal{B}}$ as a simplified alternative instead of the branch alphabet \mathcal{B} . Accordingly, we associate a label $\beta(i, \ell, j) \triangleq (i, \mathbf{d}^m, \mathbf{u}^n, \mathbf{v}^n, j)$ to $b(t) = (i, \mathbf{d}^m(t), j)$, for all $b(t) \in \mathcal{B}$, where $0 \leq \ell \leq L(i, j) - 1$, $\mathbf{d}^m \in \{0, 1\}^m$ is the m -tuple input message compatible with the realization of the branch $(i, \ell, j) \in \tilde{\mathcal{B}}$ (equivalently $(i, \mathbf{d}^m, j) \in \mathcal{B}$), and $\mathbf{u}^n, \mathbf{v}^n \in \mathbb{C}^n$ are, respectively, the associated Bob's and Eve's noiseless n -tuple observations.

In the following, we define additional notations that will be employed in Section V-A for optimizing the trellis code within the structure of the superchannel.

Definition 7 (Notation). A set of all states of the superchannel compatible with the state $i \in \mathcal{S}_e$ in the constituent E-FSMC is denoted by $\mathcal{T}_i \subseteq \mathcal{S}$. Additionally, a set of all branches of the superchannel, starting from a state $s(t-1) \in \mathcal{T}_i$, ending up with a state $s(t) \in \mathcal{T}_j$, and having noiseless outputs $\mathbf{u}^n \in \mathbb{C}^n$ and $\mathbf{v}^n \in \mathbb{C}^n$ similar to the outputs on the branch $\beta_e(i, \ell, j) \triangleq (i, \mathbf{x}^n, \mathbf{u}^n, \mathbf{v}^n, j)$ with $(i, \ell, j) \in \tilde{\mathcal{B}}_e$, is denoted by $\mathcal{T}_{ij}^{(\ell)} \subseteq \mathcal{B}$. It is important to note that each branch emanating from a particular state of the superchannel (e.g., $s(t-1) \in \mathcal{T}_i$) is from a distinct $\mathcal{T}_{ij}^{(\ell)}$ (for $\ell, j : (i, \ell, j) \in \tilde{\mathcal{B}}_e$). In Fig. 6, we sketch an exemplary trellis section of a superchannel, obtained by the concatenation of the Wolf-Ungerboeck code of rate $1/2$ depicted in Fig. 3 and the second-order E-FSMC depicted in Fig. 2. For instance, we have $\{A, B\} \in \mathcal{T}_5$ (with $5 \in \mathcal{S}_e$) and $(A, 0, 8) \in \mathcal{T}_{54}^{(0)}$ (with $(5, 0, 4) \in \mathcal{B}_e$). Also, we have $|\mathcal{T}_i| = 2$ for all $i \in \mathcal{S}_e$ and $|\mathcal{T}_{ij}^{(\ell)}| = 1$ for all $(i, \ell, j) \in \tilde{\mathcal{B}}_e$. \square

III. THEORETICAL BOUNDS

We begin this section by defining a numerical lower bound on the secrecy capacity of ISI-WTCs, as presented in [13]. We then generalize the results from [45] to (i) derive the secrecy capacity of E-FSMCs, modeling the ISI-WTCs, and (ii) extract insights from the theoretical coding strategy that achieves the secrecy capacity, which guided us in the design of a practical code achieving existing lower bounds on the secrecy capacity.

Let M_s be a random variable representing a uniformly chosen secret message m_s from an alphabet \mathcal{M}_s . Alice aims to ensure reliable and secure transmission by employing a binary code of rate $R_s \triangleq \frac{1}{N} \log |\mathcal{M}_s|$, mapping the secret message $m_s \in \mathcal{M}_s$ to a binary codeword $\mathbf{x}^N \in \{0, 1\}^N$. The reliability of Bob's decoder $\psi_N : \mathbb{C}^N \rightarrow \mathcal{M}_s$ is measured by the probability of a block error $\epsilon_N^B \triangleq \Pr(M_s \neq \psi_N(\mathbf{Y}^N))$, and the secrecy performance of the code is measured by the rate of information leakage $\epsilon_N \triangleq \frac{1}{N} I(M_s; \mathbf{Z}^N)$. With these measures,

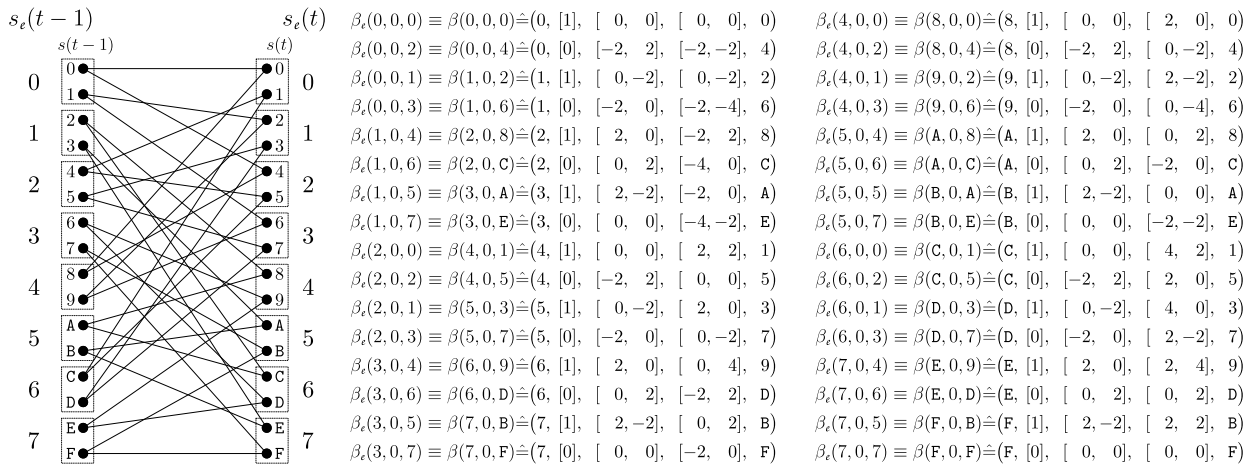


Fig. 6: Trellis section of a superchannel resulted from concatenating the trellis code depicted in Fig. 3 and the 2-nd order E-FSMC depicted in Fig. 2. Each branch of the trellis section is labeled by $\beta(i, \ell, j) \triangleq (i, d, \mathbf{u}^2, \mathbf{v}^2, j)$ for all $(i, \ell, j) \in \tilde{\mathcal{B}}$.

the reliability and secrecy criteria for the achievability of a secure rate R_s are, respectively, set to be

$$\lim_{N \rightarrow \infty} \epsilon_N^B = 0, \quad \lim_{N \rightarrow \infty} \epsilon_N = 0. \quad (4)$$

A. Constrained Secrecy Capacity

Consider an ergodic Markov source that assigns a time-invariant transition probability $p_{ij}^{(\ell)}$ to each branch $\beta_e(i, \ell, j)$ of an E-FSMC, i.e., $p_{ij}^{(\ell)} \triangleq p_{B_e(t)|S_e(t-1)}(\beta_e(i, \ell, j)|i)$ for all $(i, \ell, j) \in \tilde{\mathcal{B}}_e$. Since the Markov source and the E-FSMC are assumed to be time-invariant, a steady-state probability $\mu_i \triangleq p_{S_e(t)}(i)$ is assigned to each state $i \in \mathcal{S}_e$ of the E-FSMC. Let $Q_{ij}^{(\ell)} \triangleq \mu_i \cdot p_{ij}^{(\ell)}$ represent the probability of realizing the branch $\beta_e(i, \ell, j)$, for all $(i, \ell, j) \in \tilde{\mathcal{B}}_e$. Additionally, let $\mathbf{Q} \triangleq \{Q_{ij}^{(\ell)}\}_{(i, \ell, j) \in \tilde{\mathcal{B}}_e}$ and let $\mathcal{Q}(\tilde{\mathcal{B}}_e)$ be a polytope that includes all valid \mathbf{Q} compatible with the branch connections specified by the alphabet set $\tilde{\mathcal{B}}_e$. (See [13] and [50] for further details).

Via a straightforward generalization from [13], the constrained secrecy capacity of an n -th order E-FSMC modeling an ISI-WTC is the maximum achievable secure rate (as derived in [13, Prop. 1])⁶ obtained by optimizing over Markov inputs of finite-order

$$R_{\text{csc}}^{(n)} \triangleq \sup_{\mathbf{Q} \in \mathcal{Q}(\tilde{\mathcal{B}}_e)} \lim_{N \rightarrow \infty} \frac{1}{nN} \left(I(\mathbf{B}_e^N; \mathbf{Y}^{nN} | S_e(0)) - I(\mathbf{B}_e^N; \mathbf{Z}^{nN} | S_e(0)) \right)^+, \quad (5)$$

where the relevant maximization problem is efficiently solved using [13, Alg. 1]. Note that since the finite-state machines considered in this work are indecomposable [51] (i.e., the effect of an initial state vanishes over time), the mutual information rates are well-defined even when the initial state is unknown. Accordingly, for notational convenience, conditioning on the initial state will be omitted in the mathematical statements of the following sections.

⁶The secrecy criterion considered in [13, Prop. 1] is stronger than the weak secrecy criterion presented in (4). Consequently, all achievable secure rates in [13] are also achievable under the secrecy criterion presented in (4).

Appendix A simulates an eavesdropping scenario in a downlink transmission from a typical 256-element (16×16) phased array with an ISI-WTC. Example 1 applies [13, Alg. 1] to calculate the constrained secrecy capacity of a fourth-order E-FSMC representing this ISI-WTC. This channel model also serves as the basis for simulations in subsequent sections.

Example 1. Consider an ISI-WTC with an input alphabet $\mathcal{X} \triangleq \{-1, +1\}$, where

$$g_B[D] = (0.2360 - 0.7195i) + (0.6230 + 0.1061i)D \\ + (-0.1314 - 0.0994i)D^2, \\ g_E[D] = (0.5211 - 0.4792i) + (-0.5791 + 0.4043i)D.$$

Let $\text{SNR}_{\text{dB}}^B = \text{SNR}_{\text{dB}}^E = -4.0$, where $\text{SNR}_{\text{dB}}^u \triangleq 10 \log_{10} 1/\sigma_u^2$ for each user $u \in \{B, E\}$.⁷ The constrained secrecy capacity of the fourth-order E-FSMC modeling this ISI-WTC is $R_{\text{csc}}^{(n)}|_{n=4} = 0.121$ (bits/channel use) and the i.u.d. secure rate is $R_{\text{iud}}^{(n)}|_{n=4} = 0.013$ (bits/channel use). Additionally, refer to the corresponding curves in Fig. 9 for a wide range of $-6.0 \leq \text{SNR}_{\text{dB}}^B \leq 0$. \square

Low-density parity-check (LDPC) codes are promising candidates for secure communication over wiretap channels due to their flexible coset-based nested structure [46], powerful design tools such as density evolution [28], and reasonable encoding and decoding complexity [52]. As a result, we incorporate them into our design. Nevertheless, achieving the constrained secrecy capacity requires transmitted codewords to emulate the channel's input process that attains this bound. LDPC codes, however, lack the capability to precisely control the distribution of the generated codewords at this level. The following remark introduces a secure rate that serves as a target for single-stage LDPC codes over ISI-WTCs, and its generalization provides a benchmark for the secure rate of

⁷In the considered setup, (i) Bob operates in a low SNR regime, making it challenging to satisfy the reliability criterion; (ii) Bob's channel has a lower point-to-point capacity than Eve's channel (see Appendix A), making it challenging to satisfy the secrecy criterion; and (iii) binary phase-shift keying (BPSK) is used for inputs to simplify the presentation of the trellis code. It is important to note that neither of these considerations is strictly necessary.

LDPC codes over superchannels in the subsequent sections.

Remark 3. Let R_s be a secure rate achieved by an LDPC code having a reliability threshold above Bob's channel parameters and meeting the secrecy criterion in (4) at Eve's receiver. Then,

$$\begin{aligned} N \cdot R_s &= H(M_s) \\ &= H(M_s | \mathbf{Z}^N) + I(M_s; \mathbf{Z}^N) \\ &= H(\mathbf{X}^N | \mathbf{Z}^N) + H(M_s | \mathbf{X}^N, \mathbf{Z}^N) - H(\mathbf{X}^N | M_s, \mathbf{Z}^N) + N \cdot \varepsilon_N \\ &\stackrel{(a)}{=} H(\mathbf{X}^N) - I(\mathbf{X}^N; \mathbf{Z}^N) - H(\mathbf{X}^N | M_s, \mathbf{Z}^N) + N \cdot \varepsilon_N \\ &\leq I(\mathbf{X}^N; \mathbf{Y}^N) - I(\mathbf{X}^N; \mathbf{Z}^N) + H(\mathbf{X}^N | \mathbf{Y}^N) + N \cdot \varepsilon_N, \end{aligned} \quad (6)$$

where (a) follows from $H(M_s | \mathbf{X}^N, \mathbf{Z}^N) \leq H(M_s | \mathbf{X}^N) = 0$, and the last inequality follows from $H(\mathbf{X}^N | M_s, \mathbf{Z}^N) \geq 0$. Since Bob's decoder operates below the reliability threshold, Fano's inequality leads to $\lim_{N \rightarrow \infty} \frac{1}{N} H(\mathbf{X}^N | \mathbf{Y}^N) = 0$. Also, since the considered code satisfies $\varepsilon_N \rightarrow 0$ as $N \rightarrow \infty$, we define

$$R_s^* \triangleq \lim_{N \rightarrow \infty} \frac{1}{N} (I(\mathbf{X}^N; \mathbf{Y}^N) - I(\mathbf{X}^N; \mathbf{Z}^N))^+, \quad (7)$$

as our benchmark. According to [13, Prop. 1], R_s^* is achievable. Moreover, since the codewords generated by a randomly constructed LDPC code empirically approach a uniform distribution as $N \rightarrow \infty$, we assume that \mathbf{X}^N is generated from an i.u.d. process $\{X(t)\}_{t \in \mathbb{Z}}$. This assumption enables the numerical calculation of R_s^* using variants of the sum-product/BCJR algorithm proposed in [53]. \square

It is important to note that the benchmark in (7) *cannot* be considered a valid upper bound on the secure rates achievable by LDPC codes because (i) the relationships between codeword bits of an LDPC code are determined by the structure of the parity-check matrices and their independence cannot be guaranteed; (ii) it remains unclear whether the secrecy capacity-achieving input process for the ISI-WTC channel is block-wise independently and identically distributed (i.i.d.).

B. Secrecy Capacity of FSMCs, Modeling the ISI-WTCs

In the following, we discuss the connection between the theoretical coding strategy that achieves the secrecy capacity and our proposed two-stage coding scheme that approaches the constrained secrecy capacity. We start by extending the secrecy capacity results from [45] to E-FSMCs modeling ISI-WTCs.

Proposition 1. For any positive integer $n > \max\{\nu^B, \nu^E\}$, the secrecy capacity of an n -th order E-FSMC, modeling an ISI-WTC, under the reliability criterion in (4) and the strong secrecy criterion $N \cdot \varepsilon_N \rightarrow 0$ (as $N \rightarrow \infty$) is given by

$$C_s^{(n)} = \frac{1}{n} \sup_{p_{D^n}: D^n \perp S_e} \left(I(D^n; \mathbf{Y}^n) - I(D^n; \mathbf{Z}^n) \right)^+, \quad (8)$$

where $D(t) \in \mathcal{D}$ is an auxiliary random variable that complies with $D^n(t) \perp S_e(t)$ and the following Markov chains

$$\begin{aligned} D^n(t) &\rightarrow (\mathbf{X}^n(t), S_e(t)) \rightarrow \mathbf{Y}^n(t), \quad (\forall t \in \mathbb{Z}), \\ D^n(t) &\rightarrow (\mathbf{X}^n(t), S_e(t)) \rightarrow \mathbf{Z}^n(t), \quad (\forall t \in \mathbb{Z}). \end{aligned}$$

These Markov chains identify an auxiliary channel at the input of the E-FSMC as follows

$$\begin{aligned} p_{X^{nN} | S_e^N, D^{nN}}(\mathbf{x}^{nN} | s_e^N, \mathbf{d}^{nN}) \\ = \prod_{t=1}^N p_{X^n(t) | S_e(t), D^n(t)}(\mathbf{x}^n(t) | s_e(t), \mathbf{d}^n(t)). \end{aligned} \quad (9)$$

Proof: See Appendix B. \blacksquare

Based on the principles underlying the theoretical coding strategy that achieves the secrecy capacity (refer to Appendix B), we aim to implement the stochastic map described in (9) using an *inner*-stage trellis code (Definition 5). This code stage ensures that the uniformly distributed codewords $\{D(t)\}_{t \in \mathbb{Z}}$, generated by an *outer*-stage LDPC code, are mapped into a Markov process $\{X(t)\}_{t \in \mathbb{Z}}$, achieving the constrained secrecy capacity of the ISI-WTC. In this configuration (see Fig. 4), the i.u.d. secure rate of the resulting superchannel (Definition 6) achieves the constrained secrecy capacity of the ISI-WTC. Accordingly, we set the target secure rate for the LDPC code operating at the *outer* stage to the i.u.d. secure rate of the superchannel (per Remark 3), which, as noted, equals the constrained secrecy capacity of the constituent ISI-WTC.

IV. TWO-STAGE FACTOR GRAPH OF THE CONCATENATED CODE

In this section, we concatenate the factor graph of the superchannel (Fig. 5) with an outer LDPC code stage. We then describe the employed punctured encoding procedure and outline the modified version of the density evolution [28] for the concatenated factor graph.

Let FN, VN, and CN be the abbreviations standing for the factor nodes of a superchannel (see Fig. 5), the variable nodes, and the check nodes of an LDPC code, respectively. With a slight abuse of notation, let us denote the l -th element of the time-indexed vector $\mathbf{D}^m(t)$ with $D_l(t) \triangleq D((t-1)m+1)$ when the length of the vector is clear from the context. Given the output realizations \mathbf{y}^{nN} , the soft-output information emanating from the FNs of the superchannel is the logarithmic *a posteriori* probability (APP) ratio of the symbol $d_l(t) \in \{0, 1\}$

$$E_l(t) \triangleq \log \left(\frac{p_{D_l(t) | \mathbf{Y}^{nN}}(1 | \mathbf{y}^{nN})}{1 - p_{D_l(t) | \mathbf{Y}^{nN}}(1 | \mathbf{y}^{nN})} \right), \quad (10)$$

for all $1 \leq l \leq m$ and $1 \leq t \leq N$. Let us define $\mathcal{B}(d_l = 1) \triangleq \{(i, \mathbf{d}^m, j) \in \mathcal{B} : d(l) = 1\}$. Then, we have

$$p_{D_l(t) | \mathbf{Y}^{nN}}(1 | \mathbf{y}^{nN}) = \sum_{(i, \mathbf{d}^m, j) \in \mathcal{B}(d_l=1)} p_{B(t) | \mathbf{Y}^{nN}}(i, \mathbf{d}^m, j | \mathbf{y}^{nN}), \quad (11)$$

where $p_{B(t) | \mathbf{Y}^{nN}}(i, \mathbf{d}^m, j | \mathbf{y}^{nN})$ is calculated by running the windowed version of the BCJR algorithm [54], given the observations from the channel's output and the extrinsic information available from the outer code stage (Fig. 7). Since for $N \rightarrow \infty$ the soft-output messages $(E_l(t))_{t=1}^N$ have different statistics for each $1 \leq l \leq m$, we employ m separated LDPC subcodes as the outer code stage [35]. The normal graph of the two-stage code is depicted in Fig. 8.

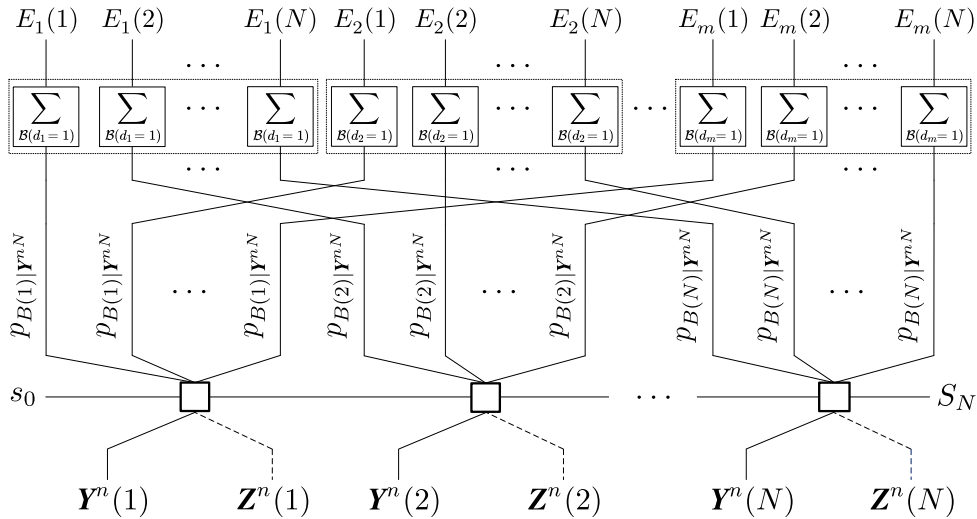


Fig. 7: Soft-output messages from FNs to VNs at Bob's decoder. (Refer to equations (10) and (11).)

A. Nested Structure and Punctured Coding

According to the equation $N \cdot \varepsilon_N = I(\mathbf{X}^N; \mathbf{Z}^N) + H(\mathbf{X}^N | M_s, \mathbf{Z}^N) - H(\mathbf{X}^N | M_s)$, the employed coding scheme should avoid a bijection between M_s and \mathbf{X}^N in order to leverage the term $H(\mathbf{X}^N | M_s) > 0$ for the cancellation of $I(\mathbf{X}^N; \mathbf{Z}^N) + H(\mathbf{X}^N | M_s, \mathbf{Z}^N)$. To accomplish this, a nested code is adopted for wiretap channels, which comprises a mother code $\mathcal{C} \subset \{0,1\}^N$ with a design rate R_d (i.e., $\dim(\mathcal{C}) = N \cdot R_d$) and a subspace $\mathcal{C}' \subset \mathcal{C}$ such that $\dim(\mathcal{C}) - \dim(\mathcal{C}') = N \cdot R_s$. The subspace \mathcal{C}' partitions the mother code \mathcal{C} into $2^{N \cdot R_s} (= |\mathcal{M}_s|)$ disjoint subcodes $\mathcal{C} \triangleq \bigcup_{i \in \mathcal{M}_s} \mathcal{C}'_i$, with $\{\mathcal{C}'_i\}_{i \in \mathcal{M}_s}$ being cosets of \mathcal{C}' . Alice encodes her secret message $m_s \in \mathcal{M}_s$, by choosing a *random* codeword from the coset $\mathcal{C}'_{i|m_s}$. Accordingly, Alice also requires a dummy message $m_r \in \mathcal{M}_r$ with $|\mathcal{M}_r| \triangleq 2^{\dim(\mathcal{C}')} to capture the local randomness required for choosing the *random* codeword from \mathcal{C}'_i . Let M_r be a random variable corresponding to a uniformly chosen dummy message m_r from \mathcal{M}_r , independent of M_s . In this setting, the non-zero term $H(\mathbf{X}^N | M_s) = H(M_r) = N \cdot R_r$, with $R_r \triangleq \frac{1}{N} \log |\mathcal{M}_r|$ representing the rate of the dummy message, ensures the non-bijective mapping required to meet the secrecy criterion.$

The mentioned nested structure is implemented in the *outer* stage using LDPC codes. Let $\mathbf{m}_s \in \{0,1\}^{K_s}$ and $\mathbf{m}_r \in \{0,1\}^{K_r}$ be the binary vectors corresponding to the secret message and the dummy message, respectively. Then, $\mathbf{m} \triangleq (\mathbf{m}_s, \mathbf{m}_r)$ denotes the message vector, which is partitioned into $m \in \mathbb{Z}$ subvectors $\{\mathbf{m}^{(l)}\}_{l=1}^m$ with $\mathbf{m}^{(l)} \triangleq (\mathbf{m}_s^{(l)}, \mathbf{m}_r^{(l)})$. For all $1 \leq l \leq m$, each subvector $\mathbf{m}^{(l)}$ is systematically encoded using the l -th LDPC subcode of rate $R_{\text{out}}^{(l)}$ and blocklength $N^{(l)} \in \mathbb{Z}$. Accordingly, the associated lengths of $\mathbf{m}^{(l)}$, $\mathbf{m}_s^{(l)}$, and $\mathbf{m}_r^{(l)}$ are respectively $N^{(l)} \cdot R_{\text{out}}^{(l)}$, $K_s \cdot \frac{N^{(l)} \cdot R_{\text{out}}^{(l)}}{\sum_{i=1}^m N^{(i)} \cdot R_{\text{out}}^{(i)}}$, and $K_r \cdot \frac{N^{(l)} \cdot R_{\text{out}}^{(l)}}{\sum_{i=1}^m N^{(i)} \cdot R_{\text{out}}^{(i)}}$, for all $1 \leq l \leq m$.

To prevent the eavesdropper from extracting secret information using the systematic part of codewords, we *puncture* the secret message subvectors $\mathbf{m}_s^{(l)}$ from output blocks of the l -th LDPC subcode for all $1 \leq l \leq m$. In our simulations,

we choose the values of $N^{(l)}$ (for $1 \leq l \leq m$) such that the blocklengths of all *punctured* subcodes become a constant integer independent of l (see Remark 7), denoted by

$$N' \triangleq N^{(l)} \cdot \left(1 - \frac{K_s \cdot R_{\text{out}}^{(l)}}{\sum_{i=1}^m N^{(i)} \cdot R_{\text{out}}^{(i)}}\right), \quad \text{for all } 1 \leq l \leq m.$$

For $q^{(l)} \triangleq (N^{(l)} - N')/N^{(l)}$ being the fraction of the *punctured* VNs in the l -th LDPC subcode, the rate of the l -th *punctured* subcode becomes $R_{\text{out}}'^{(l)} \triangleq R_{\text{out}}^{(l)}/(1 - q^{(l)})$ and the rate of the overall *punctured* outer-stage code becomes

$$R_{\text{out}}' \triangleq \frac{1}{m} \sum_{l=1}^m R_{\text{out}}'^{(l)}.$$

Let $(d_l(t))_{t=1}^{N'}$ denote the *punctured* output block from the l -th LDPC encoder for all $1 \leq l \leq m$. These m output blocks $\{(d_l(t))_{t=1}^{N'}\}_{l=1}^m$ are interleaved into N' vectors $\{\mathbf{d}^m(t)\}_{t=1}^{N'}$, where each $\mathbf{d}^m(t)$ is encoded with the superchannel for all $1 \leq t \leq N'$ (see Fig. 8). Finally, the channel observations $\mathbf{y}^{nN'}$ and $\mathbf{z}^{nN'}$ are received at Bob's and Eve's decoders, respectively.

It is crucial to apply puncturing directly to the outputs of the outer code stage *before* they are encoded by the inner trellis code (see Fig. 8). If puncturing is performed *after* encoding with the inner code stage, the memory effect of the trellis code can cause private information to leak into adjacent positions, potentially exposing it to the eavesdropper.

B. Asymptotic Analysis of the Two-Stage Turbo Decoder

An ensemble of LDPC codes is specified by a blocklength and a fixed degree distribution of the corresponding bipartite graphs. Let $\lambda_j^{(l)}$ ($\rho_j^{(l)}$) denote the fraction of edges connected to the VNs (CNs) of degree j in the l -th subcode, for $1 \leq l \leq m$. The degree distribution of the l -th subcode ensemble is represented by $(\boldsymbol{\lambda}^{(l)}, \boldsymbol{\rho}^{(l)})$, where $\boldsymbol{\lambda}^{(l)} \triangleq (\lambda_j^{(l)})_j$ and $\boldsymbol{\rho}^{(l)} \triangleq (\rho_j^{(l)})_j$. The rate of the l -th *unpunctured* subcode from this ensemble is calculated by $R_{\text{out}}^{(l)} = 1 - \left(\sum_j \rho_j^{(l)}/j\right) / \left(\sum_j \lambda_j^{(l)}/j\right)$.

Density evolution is a method for tracking the evolution of the message PDFs passing through the nodes of a factor

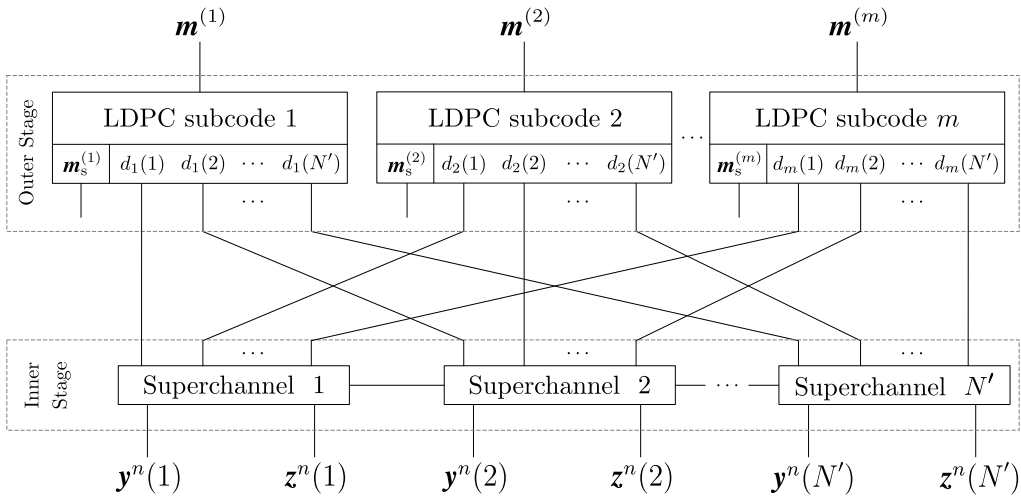


Fig. 8: Normal graph of the two-stage concatenated code, comprising a superchannel ($R_{\text{in}} = m/n$) and m LDPC subcodes as the outer stage.

graph [28]. Applying density evolution to the factor graph of a sum-product decoder enables one to asymptotically approximate the error probability of the corresponding code ensemble at each iteration. In the following, we apply density evolution to the factor graph of the concatenated code involving the sum-product decoder of the l -th *punctured* subcode.⁸ We omit the subcode index l from message PDFs for brevity of notation.

Let $f_{\text{vc}}^{(i)}(\xi)$ be the density of messages from VNs to CNs at the i -th iteration of the decoder ($i \in \mathbb{Z}$). Accordingly, the block error probability at the i -th iteration is approximated by [28]

$$e_i \triangleq \int_{-\infty}^0 f_{\text{vc}}^{(i+1)}(\xi) d\xi. \quad (12)$$

Additionally, let $f_{\text{fv}}^{(i)}(\xi)$ be the density of messages from FNs to VNs and let $f_{\text{cv}}^{(i)}(\xi)$ be the density of messages from CNs to VNs. Then, the density $f_{\text{vc}}^{(i+1)}(\xi)$ in (12) is calculated by

$$f_{\text{vc}}^{(i+1)}(\xi) = (q^{(i)} \cdot \delta(\xi) + (1 - q^{(i)}) \cdot f_{\text{fv}}^{(i)}(\xi)) * \sum_j \lambda_j^{(i)}(f_{\text{cv}}^{(i)}(\xi))^{*(j-1)},$$

where the impulse of weight $q^{(i)}$ at zero refers to the decoder's uncertainty (zero belief) about the *punctured* VNs. The density $f_{\text{cv}}^{(i+1)}(\xi)$ is calculated by evolving $f_{\text{vc}}^{(i+1)}(\xi)$ through the CNs of the LDPC decoder. This can be accomplished by defining the densities and using precomputed lookup tables as in [55], [56].

Let $\Lambda_j^{(l)} \triangleq \lambda_j^{(l)} / (j \cdot \sum_d \frac{\lambda_d}{d})$ be the fraction of VNs of degree j in the l -th subcode. Then, the density of messages from VNs to FNs is calculated by

$$f_{\text{fv}}^{(i+1)}(\xi) = \sum_j \Lambda_j^{(i)} (f_{\text{cv}}^{(i+1)}(\xi))^{*(j-1)}.$$

Finally, the density $f_{\text{vf}}^{(i+1)}(\xi)$ is derived by evolving $f_{\text{fv}}^{(i+1)}(\xi)$ through the FNs of the superchannel using Monte Carlo simu-

lations. This process involves generating a sample block $\mathbf{y}^{nN'}$,⁹ and mN' independent realizations from the density $f_{\text{vf}}^{(i+1)}(\xi)$. After evolving the realizations from $f_{\text{vf}}^{(i+1)}(\xi)$ as the extrinsic information and $\mathbf{y}^{nN'}$ as the channel observations through a windowed BCJR decoder, the density $f_{\text{fv}}^{(i+1)}(\xi)$ is estimated by a PMF using the histogram of the soft-output messages from the BCJR decoder. (See [20, Sec. IV-B] and [57].)

V. CODE DESIGN

A. Inner Trellis Code Stage

In this section, we use the design principles outlined in [35] to design a trellis code that maps the input i.u.d. process to the output Markov process, achieving the constrained secrecy capacity of the ISI-WTC. We begin by determining the desired rate for the inner trellis code.

Let $\mathbf{Q}^* \triangleq \{Q_{ij}^{*(\ell)}\}_{(i,\ell,j) \in \check{\mathcal{B}}_e}$ characterize an optimized Markov source, achieving the constrained secrecy capacity (5) of an n -th order E-FSMC specified by $\check{\mathcal{B}}_e$, and let $\{p_{ij}^{*(\ell)} \triangleq Q_{ij}^{*(\ell)} / (\sum_{\ell,j:(i,\ell,j) \in \check{\mathcal{B}}_e} Q_{ij}^{*(\ell)})\}_{(i,\ell,j) \in \check{\mathcal{B}}_e}$ represent the corresponding state transition probabilities. Additionally, let $R_d \triangleq R_{\text{in}} \cdot R'_{\text{out}}$ be the design rate of the concatenated code and let $R_{\text{in}} \triangleq m/n$ be the rate of the inner trellis code. Since the BCJR decoding complexity grows exponentially with the trellis code's input vector length m (see [35] and Remark 8), we designate the smallest values of m and n , satisfying

$$R_d < R_{\text{in}} \triangleq \frac{m}{n} \leq \frac{1}{n} \min_{(i,\ell,j) \in \check{\mathcal{B}}_e} \left(\log \frac{1}{p_{ij}^{*(\ell)}} \right), \quad (13)$$

where obeying the strict lower bound $R_{\text{in}} > R_d$ allows for the use of an outer code stage of rate $R'_{\text{out}} = R_d/R_{\text{in}}$ to implement the nested structure of the wiretap codes (Section IV-A). Additionally, the upper bound ensures the unique decodability of the trellis code. Specifically, as will be demonstrated later in this section, the main idea in designing the trellis code is to find a superchannel where $\Pr(b(t) \in \mathcal{T}_{ij}^{(\ell)} | s(t-1) \in \mathcal{T}_i)$ approaches $p_{ij}^{*(\ell)}$ for all $(i,\ell,j) \in \check{\mathcal{B}}_e$. Nevertheless, since

⁸The concentration of the decoder behavior and the zero-error threshold to the expected values over all possible graphs and cosets in the code ensemble is a direct consequence of the results presented in [20, Sec. III].

⁹First, we generate mN' i.u.d. symbols $\mathbf{d}^{mN'} \in \{0,1\}^{mN'}$. Then, we encode $\{\mathbf{d}^m(t)\}_{t=1}^{N'}$ using the superchannel to obtain $\mathbf{y}^{nN'}$ at Bob's output.

TABLE I: PARAMETERS OF THE OPTIMIZED MARKOV SOURCE, $\{Q_{ij}^{*(\ell)}\}_{(i,\ell,j) \in \check{\mathcal{B}}_e}$ AND $\{\mu_i^*\}_{i \in \mathcal{S}_e}$, CALCULATED BY [13, ALG. 1]. OPTIMAL VALUES OF $\{k_i \in \mathbb{Z}\}_{i \in \mathcal{S}_e}$, $\{\kappa_i\}_{i \in \mathcal{S}_e}$, $\{v_{ij}^{(\ell)} \in \mathbb{Z}\}_{(i,\ell,j) \in \check{\mathcal{B}}_e}$, AND $\{\check{Q}_{ij}^{(\ell)}\}_{(i,\ell,j) \in \check{\mathcal{B}}_e}$, CALCULATED BY SOLVING (14) AND (15). (EXAMPLE 2 AND EXAMPLE 3).

$\beta_e(i, \ell, j)$	$Q_{ij}^{*(\ell)}$	$v_{ij}^{(\ell)}$	$\check{Q}_{ij}^{(\ell)}$	$\beta_e(i, \ell, j)$	$Q_{ij}^{*(\ell)}$	$v_{ij}^{(\ell)}$	$\check{Q}_{ij}^{(\ell)}$	$\beta_e(i, \ell, j)$	$Q_{ij}^{*(\ell)}$	$v_{ij}^{(\ell)}$	$\check{Q}_{ij}^{(\ell)}$	$\beta_e(i, \ell, j)$	$Q_{ij}^{*(\ell)}$	$v_{ij}^{(\ell)}$	$\check{Q}_{ij}^{(\ell)}$
$\beta_e(0, 0, 0)$	0.2004	80	0.2000	$\beta_e(1, 0, 0)$	0.0040	2	0.0050	$\beta_e(2, 0, 0)$	0.0472	19	0.0475	$\beta_e(3, 0, 0)$	0.0606	24	0.0600
$\beta_e(0, 0, 1)$	0.0051	2	0.0050	$\beta_e(1, 0, 1)$	0.0001	0	0	$\beta_e(2, 0, 1)$	0.0005	0	0	$\beta_e(3, 0, 1)$	0.0006	0	0
$\beta_e(0, 0, 2)$	0.0082	3	0.0075	$\beta_e(1, 0, 2)$	0.0069	3	0.0075	$\beta_e(2, 0, 2)$	0.0011	1	0.0025	$\beta_e(3, 0, 2)$	0.0383	15	0.0375
$\beta_e(0, 0, 3)$	0.0028	1	0.0025	$\beta_e(1, 0, 3)$	0.0040	2	0.0050	$\beta_e(2, 0, 3)$	0.0009	0	0	$\beta_e(3, 0, 3)$	0.0397	16	0.0400
$\beta_e(0, 1, 0)$	0.0196	8	0.0200	$\beta_e(1, 1, 0)$	0.0007	0	0	$\beta_e(2, 1, 0)$	0.0038	2	0.0050	$\beta_e(3, 1, 0)$	0.0047	2	0.0050
$\beta_e(0, 1, 1)$	0.0005	0	0	$\beta_e(1, 1, 1)$	0.0000	0	0	$\beta_e(2, 1, 1)$	0.0000	0	0	$\beta_e(3, 1, 1)$	0.0000	0	0
$\beta_e(0, 1, 2)$	0.0008	0	0	$\beta_e(1, 1, 2)$	0.0010	0	0	$\beta_e(2, 1, 2)$	0.0002	0	0	$\beta_e(3, 1, 2)$	0.0025	1	0.0025
$\beta_e(0, 1, 3)$	0.0006	0	0	$\beta_e(1, 1, 3)$	0.0011	0	0	$\beta_e(2, 1, 3)$	0.0000	0	0	$\beta_e(3, 1, 3)$	0.0014	1	0.0025
$\beta_e(0, 2, 0)$	0.0087	4	0.0100	$\beta_e(1, 2, 0)$	0.0000	0	0	$\beta_e(2, 2, 0)$	0.0026	1	0.0025	$\beta_e(3, 2, 0)$	0.0003	0	0
$\beta_e(0, 2, 1)$	0.0089	4	0.0100	$\beta_e(1, 2, 1)$	0.0000	0	0	$\beta_e(2, 2, 1)$	0.0008	0	0	$\beta_e(3, 2, 1)$	0.0005	0	0
$\beta_e(0, 2, 2)$	0.0001	0	0	$\beta_e(1, 2, 2)$	0.0001	0	0	$\beta_e(2, 2, 2)$	0.0000	0	0	$\beta_e(3, 2, 2)$	0.0019	1	0.0025
$\beta_e(0, 2, 3)$	0.0077	3	0.0075	$\beta_e(1, 2, 3)$	0.0069	3	0.0075	$\beta_e(2, 2, 3)$	0.0022	1	0.0025	$\beta_e(3, 2, 3)$	0.0564	23	0.0575
$\beta_e(0, 3, 0)$	0.0492	20	0.0500	$\beta_e(1, 3, 0)$	0.0009	0	0	$\beta_e(2, 3, 0)$	0.0263	11	0.0275	$\beta_e(3, 3, 0)$	0.0044	2	0.0050
$\beta_e(0, 3, 1)$	0.0389	16	0.0400	$\beta_e(1, 3, 1)$	0.0011	0	0	$\beta_e(2, 3, 1)$	0.0047	2	0.0050	$\beta_e(3, 3, 1)$	0.0038	1	0.0025
$\beta_e(0, 3, 2)$	0.0003	0	0	$\beta_e(1, 3, 2)$	0.0004	0	0	$\beta_e(2, 3, 2)$	0.0002	0	0	$\beta_e(3, 3, 2)$	0.0091	4	0.0100
$\beta_e(0, 3, 3)$	0.0687	27	0.0675	$\beta_e(1, 3, 3)$	0.0099	4	0.0100	$\beta_e(2, 3, 3)$	0.0065	3	0.0075	$\beta_e(3, 3, 3)$	0.2213	88	0.2200
$\mu_0^* = 0.4204$ $k_0 = 84, \kappa_0 = 0.4200$				$\mu_1^* = 0.0369$ $k_1 = 7, \kappa_1 = 0.0350$				$\mu_2^* = 0.0972$ $k_2 = 20, \kappa_2 = 0.1000$				$\mu_3^* = 0.4456$ $k_3 = 89, \kappa_3 = 0.4450$			

each branch emanating from a state $s(t-1) \in \mathcal{T}_i$ of the superchannel must be from a distinct element of the set $\{\mathcal{T}_{ij}^{(\ell)}\}_{\ell, j: (i, \ell, j) \in \check{\mathcal{B}}_e}$ and because the input process of the superchannel is i.u.d., one can verify $\Pr(b(t) \in \mathcal{T}_{ij}^{(\ell)} | s(t-1) \in \mathcal{T}_i) \leq 2^{-m}$ for all $(i, \ell, j) \in \check{\mathcal{B}}_e$, implying the upper bound (13).

Remark 4. To ensure that the mother code (\mathcal{C} in Section IV-A) is achievable over Bob's channel, the target design rate R_d^* of the concatenated code is set to be the achievable information rate of the Markov source specified by $\mathbf{Q}^* \in \mathcal{Q}(\check{\mathcal{B}}_e)$ over Bob's channel, satisfying only the reliability criterion in (4). Therefore, according to [58], we set

$$R_d^* \triangleq \lim_{N \rightarrow \infty} \frac{I(\mathbf{X}^{nN}; \mathbf{Y}^{nN})}{nN} = \lim_{N \rightarrow \infty} \frac{I(\mathbf{B}_e^N; \mathbf{Y}^{nN})}{nN},$$

where $\{B_e(t)\}_{t \in \mathbb{Z}}$ is a branch sequence of the E-FSMC generated according to the Markov process specified by $\mathbf{Q}^* \in \mathcal{Q}(\check{\mathcal{B}}_e)$. This mutual information rate term can be efficiently calculated using variants of the sum-product/BCJR algorithm proposed in [53] due to the stationarity and ergodicity of both the E-FSMC and the input Markov process. \square

Example 2. The optimal branch probabilities of the second-order and third-order E-FSMCs, corresponding to the ISI-WTC in Example 1, violate the upper bound constraint presented in (13), even for $m = 1$ (i.e., we have $p_{ij}^{*(\ell)} > 2^{-m}$ for some $(i, \ell, j) \in \check{\mathcal{B}}_e$). By setting $n = 4$, the optimized branch probabilities of the fourth-order E-FSMC satisfy the upper bound with $m = 1$ and achieve $\lim_{N \rightarrow \infty} \frac{1}{nN} I(\mathbf{B}_e^N; \mathbf{Y}^{nN}) = 0.195$ (bits/channel use) over Bob's channel. Therefore, the target design rate of the two-stage code and the rate of the inner trellis code are set to $R_d^* = 0.195$ and $R_{in} = 1/4$, respectively. Note that the optimal values of $\{Q_{ij}^{*(\ell)}\}_{(i,\ell,j) \in \check{\mathcal{B}}_e}$ and $\{\mu_i^* \triangleq \sum_{\ell, j: (i, \ell, j) \in \check{\mathcal{B}}_e} Q_{ij}^{*(\ell)}\}_{i \in \mathcal{S}_e}$ are shown in Table I. \square

The problem of designing the trellis code stage is equivalent to optimizing the superchannel such that the i.u.d. secure rate of the superchannel approaches the constrained secrecy capac-

ity of the constituent E-FSMC. In the following, we optimize the parameters of the superchannel while assuming that the constituent E-FSMC is fixed. (Refer to Definitions 6 and 7.)

Following Definition 7, let $k_i \triangleq |\mathcal{T}_i|$ and $v_{ij}^{(\ell)} \triangleq |\mathcal{T}_{ij}^{(\ell)}|$. Accordingly, the total number of states in the superchannel becomes $|\mathcal{S}| = \sum_{i \in \mathcal{S}_e} k_i$, and the PMF $\kappa_i \triangleq k_i/|\mathcal{S}|$ is defined to be the fraction of states in \mathcal{T}_i . Additionally, the total number of branches emanating from the states in \mathcal{T}_i becomes $k_i \cdot 2^m = \sum_{\ell, j: (i, \ell, j) \in \check{\mathcal{B}}_e} v_{ij}^{(\ell)}$, and the PMF $v_{ij}^{(\ell)} \triangleq v_{ij}^{(\ell)} / (k_i \cdot 2^m)$ is defined to be the fraction of branches in $\mathcal{T}_{ij}^{(\ell)}$ over the total number of branches emanating from the states in \mathcal{T}_i . Note that the main idea in designing the desired trellis code within the superchannel is to split every state $i \in \mathcal{S}_e$ (branch $(i, \ell, j) \in \check{\mathcal{B}}_e$) of the E-FSMC into $k_i \geq 1$ states ($v_{ij}^{(\ell)} \geq 1$ branches) of the superchannel so that the following two criteria are fulfilled.

Criterion 1. Given an i.u.d. input process $\{D(t)\}_{t \in \mathbb{Z}}$, the output process $\{X(t)\}_{t \in \mathbb{Z}}$ of the trellis code should emulate the output process of the optimized Markov source characterized by $\mathbf{Q}^* \in \mathcal{Q}(\check{\mathcal{B}}_e)$. To satisfy this criterion, the probability of “being in a state from \mathcal{T}_i and taking a branch from $\mathcal{T}_{ij}^{(\ell)}$ ” is attempted to be matched on $Q_{ij}^{*(\ell)}$, for all $(i, \ell, j) \in \check{\mathcal{B}}_e$. In particular, for $\check{Q}_{ij}^{(\ell)} \triangleq \kappa_i \cdot v_{ij}^{(\ell)} = v_{ij}^{(\ell)} / (|\mathcal{S}| \cdot 2^m)$ and $\check{\mathbf{Q}} \triangleq \{\check{Q}_{ij}^{(\ell)}\}_{(i,\ell,j) \in \check{\mathcal{B}}_e}$, we attempt to match $\check{\mathbf{Q}}$ on the optimal PMF \mathbf{Q}^* by properly choosing the integer values of $\{k_i\}_{i \in \mathcal{S}_e}$ and $\{v_{ij}^{(\ell)}\}_{(i,\ell,j) \in \check{\mathcal{B}}_e}$ as follows. Following [35], we break this criterion into the following optimization problems: (i) Let $J \in \mathbb{Z}$ be the maximum number of states allowed for the superchannel in the design procedure. Also, let $\boldsymbol{\mu}^* \triangleq \{\mu_i^*\}_{i \in \mathcal{S}_e}$ (Table I) and $\boldsymbol{\kappa} \triangleq \{\kappa_i \triangleq k_i/|\mathcal{S}|\}_{i \in \mathcal{S}_e}$. The probability of realizing a state from \mathcal{T}_i is attempted to be matched on μ_i^* by solving

$$\min_{\{k_i \in \mathbb{Z}\}_{i \in \mathcal{S}_e}} \text{D}_{\text{KL}}(\boldsymbol{\kappa} || \boldsymbol{\mu}^*), \quad \text{s.t.} \quad |\mathcal{S}_e| \leq \sum_{i \in \mathcal{S}_e} k_i \leq J. \quad (14)$$

(ii) Let $\boldsymbol{\pi}_i^* \triangleq \{p_{ij}^{*(\ell)}\}_{\ell, j: (i, \ell, j) \in \check{\mathcal{B}}_e}$ (Table I) and $\mathbf{v}_i \triangleq \{v_{ij}^{(\ell)}\}_{(i,\ell,j) \in \check{\mathcal{B}}_e}$

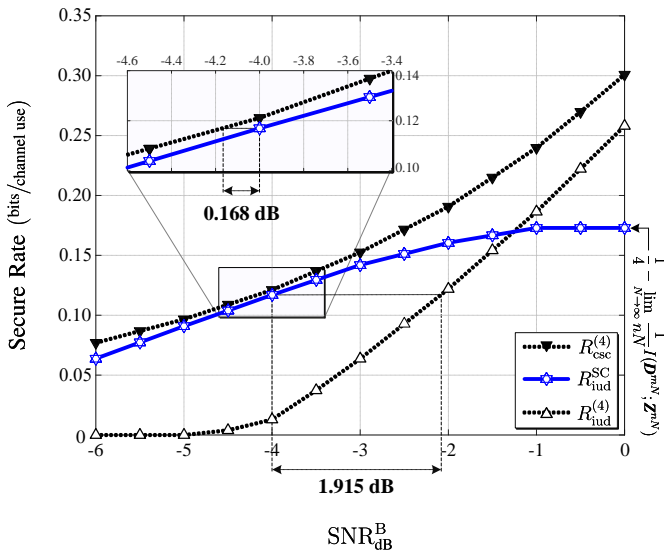


Fig. 9: The i.u.d. secure rate $R_{\text{iud}}^{(4)}$, the constrained secrecy capacity $R_{\text{csc}}^{(4)}$ of the 4-th order E-FSMC modeling the ISI-WTC in Example 1, and the i.u.d. secure rate of the superchannel $R_{\text{iud}}^{\text{SC}}$ in Table V (Example 4) for $\text{SNR}_{\text{dB}}^{\text{E}} = -4.0$. Note that the superchannel is specifically designed for operating at $\text{SNR}_{\text{dB}}^{\text{E}} = \text{SNR}_{\text{dB}}^{\text{E}} = -4.0$.

$v_{ij}^{(\ell)} / (k_i \cdot 2^m) \}_{\ell, j: (i, \ell, j) \in \tilde{\mathcal{B}}_e}$ for all $i \in \mathcal{S}_e$. Given the PMF vector κ derived from solving (14), the probability of realizing a branch within $\mathcal{T}_{ij}^{(\ell)}$ from a state in \mathcal{T}_i is attempted to be matched on $p_{ij}^{*(\ell)}$ by solving

$$\begin{aligned} \min_{\{v_{ij}^{(\ell)} \in \mathbb{Z}\}_{(i, \ell, j) \in \tilde{\mathcal{B}}_e, i \in \mathcal{S}_e}} \quad & \sum \kappa_i \cdot \text{D}_{\text{KL}}(\mathbf{v}_i || \boldsymbol{\pi}_i^*), \\ \text{s.t.} \quad & \sum_{\ell, j: (i, \ell, j) \in \tilde{\mathcal{B}}_e} v_{ij}^{(\ell)} = k_i \cdot 2^m \quad (\text{for all } i \in \mathcal{S}_e), \\ & \sum_{\ell, j: (i, \ell, j) \in \tilde{\mathcal{B}}_e} v_{ij}^{(\ell)} = \sum_{s, \ell: (s, \ell, i) \in \tilde{\mathcal{B}}_e} v_{si}^{(\ell)} \quad (\text{for all } i \in \mathcal{S}_e). \end{aligned} \quad (15)$$

A superchannel with the optimal values of $\{k_i\}_{i \in \mathcal{S}_e}$ and $\{v_{ij}^{(\ell)}\}_{(i, \ell, j) \in \tilde{\mathcal{B}}_e}$, vanishing the objective functions of (14) and (15) guarantees Criterion 1.¹⁰

Example 3. Following Example 2, the optimal values of k_i , $\kappa_i \triangleq k_i / |\mathcal{S}|$ for all $i \in \mathcal{S}_e$, and $v_{ij}^{(\ell)}$, $\check{Q}_{ij}^{(\ell)} \triangleq v_{ij}^{(\ell)} / (|\mathcal{S}| \cdot 2^m)$ for all $(i, \ell, j) \in \tilde{\mathcal{B}}_e$, are shown in Table I, for $J = 200$. \square

Criterion 2. The i.u.d. secure rate of the superchannel,

$$R_{\text{iud}}^{\text{SC}} \triangleq \lim_{N \rightarrow \infty} \frac{1}{nN} \left(I(\mathbf{D}^{mN}; \mathbf{Y}^{nN}) - I(\mathbf{D}^{mN}; \mathbf{Z}^{nN}) \right)^+, \quad (16)$$

should approach the constrained secrecy capacity of the constituent n -th order E-FSMC $R_{\text{csc}}^{(n)}$ at the required SNR value. To fulfill this criterion, among all branch connections of the superchannel that meet the optimal values of $\{k_i\}_{i \in \mathcal{S}_e}$ and $\{v_{ij}^{(\ell)}\}_{(i, \ell, j) \in \tilde{\mathcal{B}}_e}$, we choose the one that achieves the maximum i.u.d. secure rate $R_{\text{iud}}^{\text{SC}}$ using ordinal optimization [59].

Example 4. Table V in Appendix C depicts the branch connections of a superchannel, satisfying the optimal values

¹⁰The inaccuracy in approximating $\mathbf{Q}^* \in \mathcal{Q}(\tilde{\mathcal{B}}_e)$ with $\check{\mathbf{Q}}$ can be made arbitrarily small by choosing the number of allowed states for the superchannel ($J \in \mathbb{Z}$) sufficiently large.

of $\{k_i\}_{i \in \mathcal{S}_e}$ and $\{v_{ij}^{(\ell)}\}_{(i, \ell, j) \in \tilde{\mathcal{B}}_e}$ as given in Table I. These connections were determined using a randomized search with ordinal optimization. For the SNR values of Example 1, the i.u.d. secure rate of the resulting superchannel is $R_{\text{iud}}^{\text{SC}} = 0.117$ (bits/channel use), while the reference Markov source specified by \mathbf{Q}^* achieves $R_{\text{csc}}^{(n)}|_{n=4} = 0.121$ (bits/channel use). Fig. 9 illustrates the gain of the trellis code at $\text{SNR}_{\text{dB}}^{\text{E}} = -4.0$ and $-6.0 \leq \text{SNR}_{\text{dB}}^{\text{E}} \leq 0$. Note the superchannel achieves its best performance at the required SNR value, i.e., $\text{SNR}_{\text{dB}}^{\text{E}} = -4.0$, compared with the constrained secrecy capacity. As shown in Fig. 9, the i.u.d. secure rate of the superchannel converges to $R_{\text{iud}}^{\text{SC}} = 0.25 - \lim_{N \rightarrow \infty} \frac{1}{nN} I(\mathbf{D}^{mN}; \mathbf{Z}^{nN})$ as $\text{SNR}_{\text{dB}}^{\text{E}}$ exceeds a certain threshold where $\lim_{N \rightarrow \infty} \frac{1}{nN} I(\mathbf{D}^{mN}; \mathbf{Y}^{nN}) = 0.25$ (bits/channel use). This occurs because the mutual information rate of the users over the superchannel is limited by the rate of the trellis code ($R_{\text{in}} = 1/4$). To overcome this limitation, one could increase the rate of the trellis code by choosing a larger value of $m \in \mathbb{Z}$ that satisfies (13). However, the trade-off for this improvement is a larger outer code stage, a larger superchannel, and a more complex decoder. \square

Remark 5. Assigning the bit values from $\{0, 1\}^m$ to \mathbf{d}^m on each branch $(i, \mathbf{d}^m, j) \in \mathcal{B}$ of the superchannel drastically affects the performance of the outer code in terms of the block error probability. Accordingly, the final step in establishing the connection between the superchannel and the outer code stage is assigning the optimal values to $\mathbf{d}^m \in \{0, 1\}^m$ toward minimizing the block error probability of Bob's decoder. By considering a multi-stage decoder as [60] in Fig. 10, determining the values of \mathbf{d}^{l-1} ($1 \leq l \leq m$) ensures the performance of the l -th LDPC decoder depends only on the assigned bit values to $d(l)$ [35]. Therefore, starting with $l = 1$, we search for the optimal bit values of $d(l)$ such that the l -th BCJR decoder in Fig. 10 attains the lowest probability of error at the first iteration, assuming that the messages $(\mathbf{m}^{(1)}, \dots, \mathbf{m}^{(l-1)})$ have been successfully decoded. Table V in Appendix C presents the assigned bit values to $d \in \{0, 1\}$ on branches of the superchannel in Example 4. \square

B. Outer LDPC Code Stage

In this section, we estimate the rate of information leakage using a numerical upper bound. Then, we optimize the degree distributions of the outer LDPC subcodes to reduce the estimated upper bound. We begin with the following remark, which considers an auxiliary receiver terminal (cf. [39]) whose decoding block error probability is used to derive this bound.

Remark 6. Consider a fictitious receiver terminal that observes through Eve's channel and has perfect knowledge about the secret message. This receiver is referred to as "Frank". Let ϵ_N^{F} be the block error probability of Frank's decoder, trying to recover M_r through observing M_s and \mathbf{Z}^N . Indeed, Fano's inequality implies $H(M_r | M_s, \mathbf{Z}^N) \leq 1 + \epsilon_N^{\text{F}} \cdot K_r$. \square

Lemma 1. Consider a concatenated code as in Fig. 8 with the blocklength nN' , the dummy message rate R_r , and the block error probability $\epsilon_{nN'}^{\text{F}}$ at Frank's decoder. The rate of

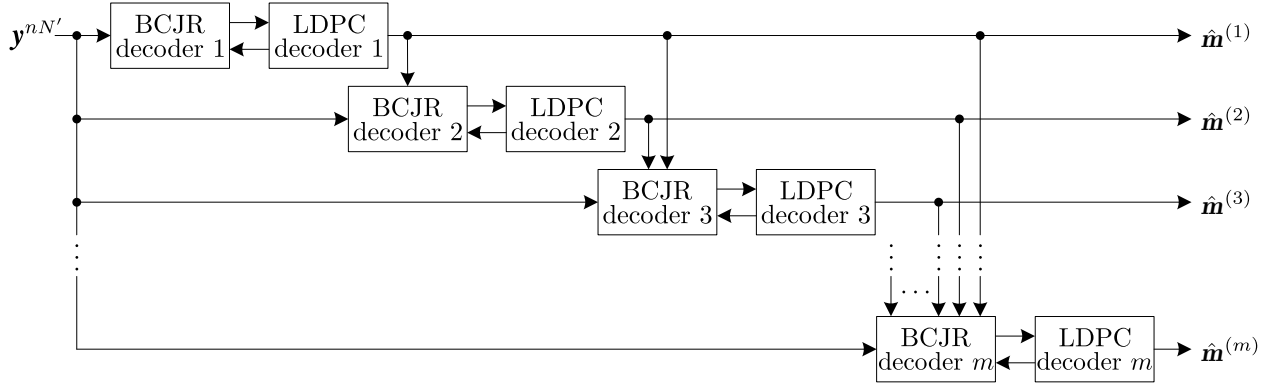


Fig. 10: Multi-stage decoder for estimating $\mathbf{m}^{(l)}$, assuming that the symbols $(\mathbf{m}^{(1)}, \dots, \mathbf{m}^{(l-1)})$ are successfully decoded without error ($1 \leq l \leq m$).

information leakage achieved by this code over an ISI-WTC is upper-bounded by

$$\varepsilon_{nN'} \leq \frac{I(\mathbf{D}^{mN'}; \mathbf{Z}^{nN'})}{nN'} - (1 - \epsilon_{nN'}^F) \cdot R_r + \frac{1}{nN'}. \quad (17)$$

Proof. We have

$$\begin{aligned} nN' \cdot \varepsilon_{nN'} &\triangleq H(M_s) - H(M_s | \mathbf{Z}^{nN'}) \\ &= K_s - H(\mathbf{D}^{mN'} | \mathbf{Z}^{nN'}) - H(M_s | \mathbf{D}^{mN'}, \mathbf{Z}^{nN'}) \\ &\quad + H(\mathbf{D}^{mN'} | M_s, \mathbf{Z}^{nN'}) \\ &\stackrel{(a)}{\leq} K_s - H(\mathbf{D}^{mN'}) + I(\mathbf{D}^{mN'}; \mathbf{Z}^{nN'}) - H(M_s | \mathbf{D}^{mN'}, \mathbf{Z}^{nN'}) \\ &\quad + \epsilon_{nN'}^F \cdot K_r + 1 \\ &\stackrel{(b)}{=} K_s - H(M_s, M_r) - H(\mathbf{D}^{mN'} | M_s, M_r) \\ &\quad + H(M_s, M_r | \mathbf{D}^{mN'}) + I(\mathbf{D}^{mN'}; \mathbf{Z}^{nN'}) - H(M_s | \mathbf{D}^{mN'}) \\ &\quad + \epsilon_{nN'}^F \cdot K_r + 1 \\ &\stackrel{(c)}{=} H(M_s | \mathbf{D}^{mN'}) + H(M_r | \mathbf{D}^{mN'}, M_s) + I(\mathbf{D}^{mN'}; \mathbf{Z}^{nN'}) \\ &\quad - H(M_s | \mathbf{D}^{mN'}) - (1 - \epsilon_{nN'}^F) \cdot K_r + 1 \\ &\stackrel{(d)}{=} I(\mathbf{D}^{mN'}; \mathbf{Z}^{nN'}) - (1 - \epsilon_{nN'}^F) \cdot K_r + 1, \end{aligned}$$

where (a) is deduced from $H(\mathbf{D}^{mN'} | M_s, \mathbf{Z}^{nN'}) = H(M_r | M_s, \mathbf{Z}^{nN'}) \leq 1 + K_r \cdot \epsilon_{nN'}^F$ in Remark 6, (b) relies on $H(M_s | \mathbf{D}^{mN'}, \mathbf{Z}^{nN'}) = H(M_s | \mathbf{D}^{mN'})$, (c) results from $H(M_s, M_r) = K_s + K_r$ and $H(\mathbf{D}^{mN'} | M_s, M_r) = 0$, and (d) follows from the fact that the dummy message M_r is systematically available in the punctured codewords $\mathbf{D}^{mN'}$, implying $H(M_r | \mathbf{D}^{mN'}, M_s) \leq H(M_r | \mathbf{D}^{mN'}) = 0$. \square

The term $I(\mathbf{D}^{mN'}; \mathbf{Z}^{nN'})/(nN')$ in (17) can be efficiently calculated using variants of the sum-product/BCJR algorithm [53] as $N' \rightarrow \infty$. Moreover, in the design procedure, the asymptotic error probability of Frank's decoder ($\epsilon^F \triangleq \lim_{N' \rightarrow \infty} \epsilon_{nN'}^F$) is approximated by applying the following modifications to the density evolution algorithm. (i) Since Frank's and Eve's observations are identical (Remark 6), to evolve $f_{\text{vf}}^{(z)}(\xi)$ through the FNs of Frank's decoder, we use Eve's observations $\mathbf{z}^{nN'}$ in the Monte Carlo step instead of Bob's observations $\mathbf{y}^{nN'}$. Let us denote the resulting density by $f_{\text{fv}}^{(z)}(\xi)$. (ii) Since Frank possesses perfect knowledge about the secret message (Remark 6), we set the density of messages

from FNs to VNs as a probabilistic mixture of the density $f_{\text{fv}}^{(z)}(\xi)$ and an impulse at $+\infty$ with the weight of $q^{(l)}$.¹¹ Thus, the density of messages from VNs to CNs of Frank's decoder is calculated by

$$\begin{aligned} f_{\text{vc}}^{(z+1)}(\xi) &= (q^{(l)} \cdot \delta(\xi - \infty) + (1 - q^{(l)}) \cdot f_{\text{fv}}^{(z)}(\xi)) \\ &\quad * \sum_j \lambda_j^{(l)}(f_{\text{cv}}^{(z)}(\xi))^{*(j-1)}, \end{aligned}$$

and the block error probability at the i -th iteration of Frank's decoder is approximated by

$$e_i^F = \int_{-\infty}^0 f_{\text{vc}}^{(z+1)}(\xi) d\xi.$$

The asymptotic error probability of Frank's decoder (ϵ^F) is estimated by $\tilde{\epsilon}^F \triangleq e_{\iota_{\max}}^F$, where $\iota_{\max} \in \mathbb{Z}$ represents the maximum number of allowed iterations or the iteration at which a stopping criterion is met. Accordingly, we estimate the asymptotic rate of information leakage by

$$\tilde{\epsilon} \triangleq \lim_{N' \rightarrow \infty} \tilde{\epsilon}_{nN'} = \lim_{N' \rightarrow \infty} \frac{I(\mathbf{D}^{mN'}; \mathbf{Z}^{nN'})}{nN'} - (1 - \tilde{\epsilon}^F) \cdot R_r. \quad (18)$$

Since Frank is allowed to use a more powerful decoder, we have $\epsilon^F \leq \tilde{\epsilon}^F$; hence, due to (17), the estimation in (18) presents an upper bound $\lim_{N' \rightarrow \infty} \varepsilon_{nN'} \leq \tilde{\epsilon}$.

Let $q \triangleq (\sum_{l=1}^m N^{(l)} - mN') / \sum_{l=1}^m N^{(l)}$ denote the fraction of all punctured VNs in the outer code stage. According to the employed puncturing policy (Section IV-A), the secure rate of the concatenated code is determined by

$$\begin{aligned} R_s &= \frac{K_s}{nN'} = \frac{\sum_{l=1}^m N^{(l)} - mN'}{nN'} = \frac{\sum_{l=1}^m N^{(l)} - mN'}{mN'} \cdot \frac{m}{n} \\ &= \frac{q}{1-q} \cdot R_{\text{in}}. \end{aligned} \quad (19)$$

Throughout the design procedure, we fix the secure rate by applying a fixed value for q .

We attempt to reduce the rate of information leakage by minimizing the estimated upper bound in (18). For a suffi-

¹¹Recall that $q^{(l)}$ represents the fraction of VNs carrying the secret message at the l -th LDPC subcode. Consequently, the impulse of weight $q^{(l)}$ at $+\infty$ appropriately captures Frank's perfect knowledge about the secret message.

ciently small value of $\tilde{\epsilon}^F > 0$, we have

$$\begin{aligned}\tilde{\epsilon} &= \lim_{N \rightarrow \infty} \frac{I(\mathbf{D}^{mN}; \mathbf{Z}^{nN})}{nN} - R_t \\ &= \lim_{N \rightarrow \infty} \frac{I(\mathbf{D}^{mN}; \mathbf{Y}^{nN})}{nN} + R_s - R_d.\end{aligned}\quad (20)$$

Accordingly, for a fixed value of the secure rate and a fixed superchannel, minimizing the rate of information leakage is equivalent to the well-known problem of maximizing the design rate of the *punctured* LDPC codes. In the following, we determine the target design rate of the outer code stage and allocate the resulting target rate among the constituent subcodes.

By choosing the number of allowed states for the superchannel sufficiently large (Section V-A), the information rate term $\frac{1}{nN} I(\mathbf{D}^{mN}; \mathbf{Y}^{nN})$ over the superchannel (with $\{D(t)\}_{t \in \mathbb{Z}}$ being an i.u.d. sequence) approaches $\frac{1}{nN} I(\mathbf{B}_e^N; \mathbf{Y}^{nN})|_{\mathbf{Q}=\mathbf{Q}^*}$ over the ISI-WTC as $N \rightarrow \infty$. Therefore, following Remark 4, we set

$$R_d^* = \lim_{N \rightarrow \infty} \frac{I(\mathbf{D}^{mN}; \mathbf{Y}^{nN})}{nN}.\quad (21)$$

Following Remark 3, by setting $R_s = R_s^*$ (where $R_s^* = R_{\text{iud}}^{\text{SC}}$ for an LDPC code operating over the superchannel) and using the expression for $R_{\text{iud}}^{\text{SC}}$ in (16), the asymptotic upper bound on the rate of information leakage in (20) becomes

$$\begin{aligned}\tilde{\epsilon} &= \lim_{N \rightarrow \infty} \frac{I(\mathbf{D}^{mN}; \mathbf{Z}^{nN})}{nN} + R_{\text{iud}}^{\text{SC}} - R_d \\ &= \lim_{N \rightarrow \infty} \frac{I(\mathbf{D}^{mN}; \mathbf{Y}^{nN})}{nN} - R_d.\end{aligned}$$

Hence, achieving the design rate $R_d = R_d^*$ as presented in (21) is a sufficient (though not necessary) condition to guarantee the weak secrecy criterion for all secure rates $R_s \leq R_{\text{iud}}^{\text{SC}}$.

Due to (21), the target design rate of the *punctured* outer code stage is set to

$$R_{\text{out}}^* \triangleq \frac{R_d^*}{R_{\text{in}}} = \lim_{N \rightarrow \infty} \frac{I(\mathbf{D}^{mN}; \mathbf{Y}^{nN})}{mN}.$$

Also, according to $R_{\text{out}}^* \triangleq \frac{1}{m} \sum_{l=1}^m R_{\text{out}}^{*(l)}$ and

$$\begin{aligned}I\left(\left(\mathbf{D}^m(t)\right)_{t=1}^N; \mathbf{Y}^{nN}\right) \\ = \sum_{l=1}^m I\left(\left(D_l(t)\right)_{t=1}^N; \mathbf{Y}^{nN} \left| \left(D_1(t) \cdots D_{l-1}(t)\right)_{t=1}^N\right.\right),\end{aligned}$$

we set the target design rate of the l -th *punctured* subcode to be the achievable rate of Bob's decoder, trying to reliably estimate $\mathbf{m}^{(l)}$ from observing \mathbf{y}^{nN} and $(d_1(t) \cdots d_{l-1}(t))_{t=1}^N$

$$R_{\text{out}}^{*(l)} \triangleq \lim_{N \rightarrow \infty} \frac{1}{N} I\left(\left(D_l(t)\right)_{t=1}^N; \mathbf{Y}^{nN} \left| \left(D_1(t) \cdots D_{l-1}(t)\right)_{t=1}^N\right.\right),\quad (22)$$

where $\{D_l(t)\}_{t \in \mathbb{Z}}$ is an i.u.d. sequence for all $1 \leq l \leq m$.¹² Using the results from [58] and the assumptions made in the multi-stage decoder depicted in Fig. 10, it is straight-

¹²Choosing the target rate for the l -th *unpunctured* subcode involves determining the value of $q^{(l)}$ for $1 \leq l \leq m$. Under the constraint $\frac{1}{m} \sum_{l=1}^m q^{(l)} = q$, the code designer is free to choose $q^{(l)}$ ($1 \leq l \leq m$) for balancing the reliability performance of LDPC subcodes by allocating smaller values of $q^{(l)}$ to subcodes with weaker reliability performance.

TABLE II: OPTIMIZED VN SIDE DEGREE DISTRIBUTIONS OF THE OUTER LDPC CODE STAGE.

j	$\lambda_j^{(1)}$	$\rho_j^{(1)}$
2	0.18212	0
3	0.00176	0.266
4	0.34291	0
5	0.47049	0
6	0.00073	0
7	0.00027	0
8	0.00015	0
9	0.00011	0
10	0.00008	0
11	0.00007	0.166
12	0.00006	0
13	0.00005	0.102
14	0.00004	0.102
19	0.00003	0.133
20	0.00003	0
21	0.00003	0.333
32	0.00003	0
33	0.00003	0
34	0.00003	0
44	0.00002	0
45	0.00002	0
		$R_{\text{out}}^{(1)} = 0.5277$

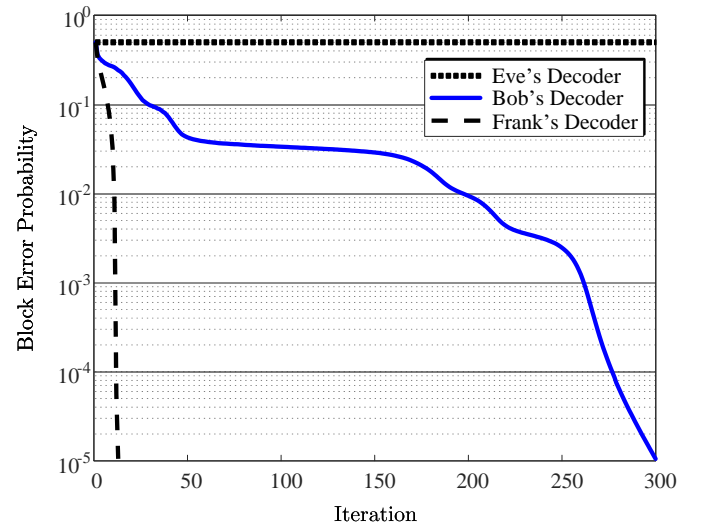


Fig. 11: The average asymptotic performance of Bob's, Eve's, and Frank's decoders, as estimated using density evolution over 100 randomly generated codewords of length 10^5 .

forward to verify that $R_{\text{out}}^{*(l)}$ is achievable for the l -th subcode under the reliability criterion specified in (4) for all $1 \leq l \leq m$. Consequently, we maximize the rate of the l -th *punctured* subcode $R_{\text{out}}^{*(l)}$ by optimizing the degree distributions $(\lambda^{(l)}, \rho^{(l)})$ to approach $R_{\text{out}}^{*(l)}$ —assuming that the codewords $(d_1(t) \cdots d_{l-1}(t))_{t=1}^N$ are successfully decoded (see Fig. 10).

Example 5. Following Example 2, since the inner trellis code has $R_{\text{in}} = 1/4$ (i.e., $m = 1$), a single LDPC code was employed as the outer stage. By using the superchannel in Table V along with the optimized degree distributions of the outer LDPC code depicted in Table II, the secrecy criterion in (4) was met at a secure rate of $R_s = 0.1100$, which is 0.42 dB away from the constrained secrecy capacity $R_{\text{csc}}^{(4)} = 0.121$ (bits/channel use). According to (19), we fixed the secure rate at $R_s = 0.1100$ by setting the fraction of the punctured VNs to $q = 0.3056$. The optimized degree distributions in Table II have an *unpunctured* rate $R_{\text{out}}^{(1)} = 0.5277$ and a *punctured* rate $R'_{\text{out}} = R_{\text{out}}^{*(1)} \triangleq R_{\text{out}}^{(1)} / (1 - q) = 0.7598$. Due to $\lim_{N \rightarrow \infty} \frac{1}{nN} I(\mathbf{D}^{mN}; \mathbf{Z}^{nN}) = 0.080$ (bits/channel use), $R_d \triangleq R_{\text{in}} \cdot R'_{\text{out}} = 0.1900$, and the upper bound in (18), the rate of information leakage is upper bounded by $\tilde{\epsilon} < 10^{-5}$.

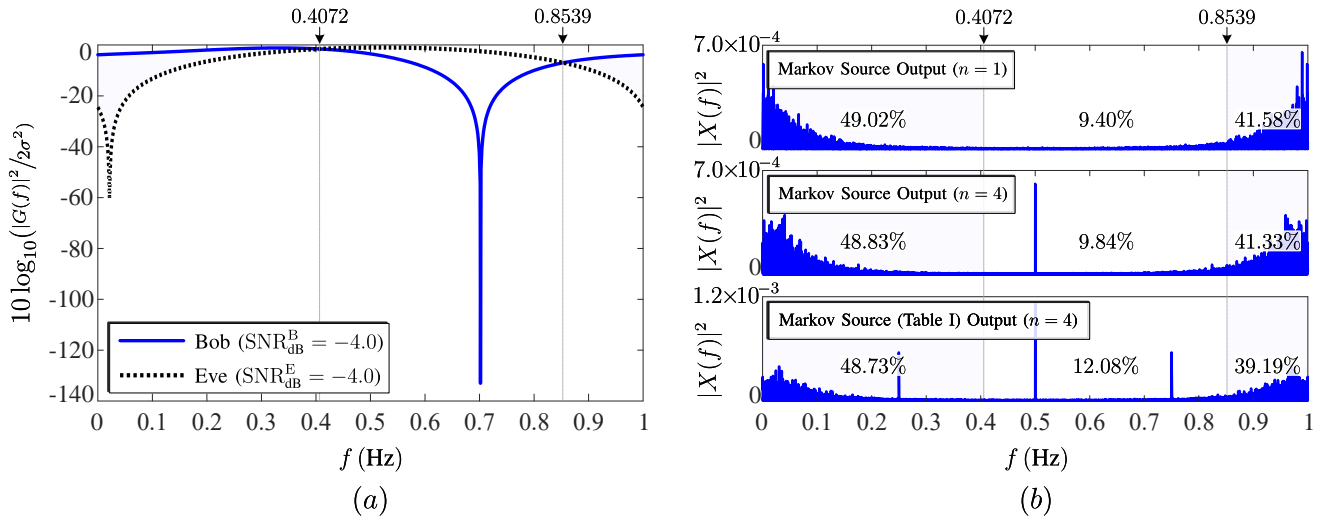


Fig. 12: (a): Gain-to-noise power spectrum ratios of Bob's and Eve's point-to-point channels in dB/Hz. (b): Power spectra of sequences produced by Markov sources optimized for the 1-st order and 4-th order E-FSMCs representing the considered ISI-WTC, and the power spectrum of a sequence generated by the Markov source specified in Table I, satisfying the upper bound constraint in (13).

We estimated the asymptotic error probabilities of sum-product decoders at Bob's, Eve's, and Frank's receivers by running the modified density evolution algorithm for 100 randomly generated codewords of length 10^5 .¹³ The average error probabilities at each iteration are depicted in Fig. 11. \square

VI. FINITE BLOCKLENGTH REGIME

We first provide remarks concerning the finite blocklength code construction procedure, then analyze the spectral properties of the codewords generated by the designed trellis code, and finally evaluate the reliability and secrecy performance of the two-stage code in the finite blocklength regime.

Careful consideration is required when specifying $N^{(l)}$ ($1 \leq l \leq m$) to ensure the output blocks of all punctured LDPC subcodes have length N' . The following remark clarifies this.

Remark 7. For fixed values of R_s , R_{in} , and R'_{out} (for all $1 \leq l \leq m$), we begin by choosing the value of N' , determining the length of the codewords transmitted over the channel, nN' . Next, we calculate $K_s \triangleq nN' \cdot R_s$ and $K_r \triangleq nN' \cdot (R_d - R_s)$, where $R_d \triangleq R_{in} \cdot R'_{out}$ and $R'_{out} \triangleq \frac{1}{m} \sum_{l=1}^m R'_{out}{}^{(l)}$. As described in Section IV-A, the length of the secret message block $\mathbf{m}_s^{(l)}$ in the l -th subcode ($\triangleq N^{(l)} - N'$) is calculated as $K_s \cdot \frac{N^{(l)} \cdot R'_{out}{}^{(l)}}{\sum_{l=1}^m N^{(l)} \cdot R'_{out}{}^{(l)}}$. Using $N^{(l)} \cdot R'_{out}{}^{(l)} = N' \cdot R'_{out}{}^{(l)}$ and $\sum_{l=1}^m N^{(l)} \cdot R'_{out}{}^{(l)} = K_s + K_r$, the blocklength of the l -th unpunctured subcode is given by

$$N^{(l)} = N' + \frac{K_s \cdot N' \cdot R'_{out}{}^{(l)}}{K_s + K_r},$$

for all $1 \leq l \leq m$. \square

The multi-stage decoder shown in Fig. 10 facilitates the code design process. However, the decoder itself comprises

¹³Given that the concentration statement for error probability depends on the input sequence in channels with independent memory [20], and that the density evolution involves a Monte Carlo step, we approximate the asymptotic performance of decoders at each iteration by averaging the estimated error probabilities across multiple input sequences.

only two stages: a windowed BCJR decoder for the trellis code stage and a sum-product decoder for the overall LDPC code stage, encompassing all subcodes [35]. In the following, we outline the construction of the overall LDPC code stage.

For $1 \leq l \leq m$, let $\mathbf{H}^{(l)} = (\mathbf{h}_1^{(l)} \mathbf{h}_2^{(l)} \cdots \mathbf{h}_{N^{(l)}}^{(l)})$ denote the parity-check matrix of the l -th LDPC subcode with $\mathbf{h}_t^{(l)}$ representing the t -th column of $\mathbf{H}^{(l)}$. Also, let $N'' \triangleq \max_{\ell} N^{(\ell)}$. For all $1 \leq l \leq m$ in which $N^{(l)} < N''$, we set $\mathbf{h}_t^{(l)} \triangleq \mathbf{0}$ for column indices $N^{(l)} < t \leq N''$. We then define

$$\mathbf{H}_t \triangleq \begin{pmatrix} \mathbf{h}_t^{(1)} & \mathbf{0} & \cdots & \mathbf{0} \\ \mathbf{0} & \mathbf{h}_t^{(2)} & \cdots & \mathbf{0} \\ \vdots & \vdots & \ddots & \vdots \\ \mathbf{0} & \mathbf{0} & \cdots & \mathbf{h}_t^{(m)} \end{pmatrix}, \quad (\text{for } 1 \leq t \leq N'').$$

The parity-check matrix of the overall LDPC code is obtained by interleaving the columns of the subcode parity-check matrices as $(\mathbf{H}_1 \mathbf{H}_2 \cdots \mathbf{H}_{N''})$ and removing any all-zero columns. See Fig. 8 and refer to [35, Sec. V-D] for further details.

Remark 8. In our simulations, instead of iterating the decoding algorithm between the inner and outer code stages at each iteration, we apply BCJR decoding at the inner stage only once every 5 – 10 iterations of message passing within the outer stage. This approach improves the convergence characteristics of the turbo decoder for short blocklengths while providing substantial computational savings for large blocklengths, as performing one iteration of BCJR decoding for a trellis code of rate m/n has a complexity of order $\mathcal{O}(N' \cdot |\mathcal{S}| \cdot 2^m)$. \square

A. Spectral Properties

In the considered setup, Bob's channel has a lower point-to-point unconstrained capacity compared to Eve's channel, as detailed in Appendix A. However, when examining the gain-to-noise power spectrum ratio ($|G(f)|^2/2\sigma^2$) for both channels, we observe favorable frequencies for Bob where his channel has a higher gain-to-noise ratio than Eve's channel (Fig. 12(a)). By optimizing the input Markov sources, as

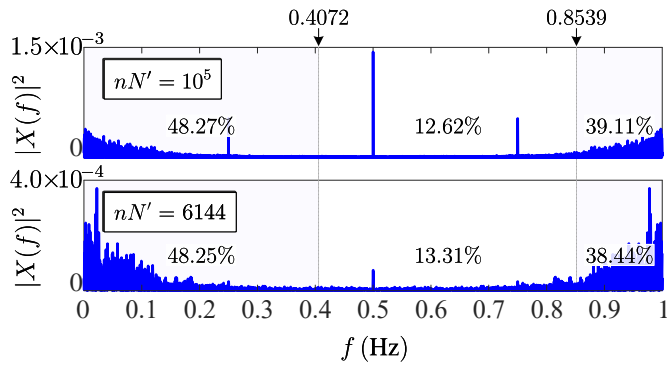


Fig. 13: Power spectra of sample codewords generated by the inner trellis code specified in Table V ($n = 4$) using LDPC codewords of lengths $N' \in \{25000, 1536\}$ as inputs.

demonstrated in [13], these spectral discrepancies can be exploited to enable positive secure rates, as done in Example 1 (see Fig. 9). Fig. 12(b) presents the normalized power spectra of sequences of length 10^5 generated by Markov sources optimized for the first-order and fourth-order E-FSMCs representing the considered ISI-WTC. These Markov sources effectively allocate over 90% of the total available power to frequency ranges where Bob's gain-to-noise ratio surpasses Eve's. Notice that the Markov sources shown in the upper- and middle-right subplots violate the upper bound constraint in (13). In contrast, the lower-right subplot depicts the normalized power spectrum of a sequence generated by the optimized Markov source in Table I, having $n = 4$ and satisfying (13).

As shown in the middle and lower subplots of Fig. 12(b), unintended impulses appear in the spectra of sequences generated by optimized Markov sources for $n = 4$ (and $n > 1$ in general). In an E-FSMC of order n , the branch process $\{b_\epsilon(t)\}_{t \in \mathbb{Z}}$ and, consequently, the block-output process $\{x^n(t)\}_{t \in \mathbb{Z}}$ are controlled by the input Markov source. However, the Markov source does not influence the internal structure within each block, $(x(n(t-1)+1), \dots, x(nt))$. We conjecture that these observed impulses originate from this internal structure, which fails to conform to the desired spectral characteristics of the optimized Markov source.¹⁴ Note the two additional impulses observed in the lower subplot of Fig. 12(b) result from a higher likelihood of patterns $(0, 0, 1, 0)$, $(0, 1, 0, 0)$, $(0, 1, 1, 0)$, $(1, 0, 0, 1)$, $(1, 0, 1, 1)$, and $(1, 1, 0, 1)$ in the output. Indeed, the increased occurrence of these patterns arises from adhering to the upper bound constraint in (13), which is violated by the Markov source used in the middle subplot.

Fig. 13 illustrates the normalized power spectra of sample codewords generated by the inner trellis code specified in Table V, using LDPC codewords of lengths 25000 and 1536 as inputs.¹⁵ As illustrated, even for short blocklengths, the codewords produced by the designed trellis code effectively

¹⁴To verify the conjecture, each length- n block ($\in \mathcal{X}^n$) in the generated sequence was assigned a corresponding single-letter variable with an alphabet size $|\mathcal{X}|^n$. The spectrum of the resulting sequence no longer exhibits unintended impulses and reasonably aligns with that of sequences generated by the optimized Markov source with $n = 1$, supporting the conjecture.

¹⁵Choosing $N' = 1536$, resulting in a blocklength of $nN' = 6144$, is based on the 5G New Radio (NR) specifications in 3GPP TS 38.212 [61], which define LDPC codes for error correction over the physical downlink shared channel.

TABLE III: OPTIMIZED VN SIDE DEGREE DISTRIBUTIONS OF THE OUTER LDPC CODE STAGE FOR $R_s = 0.0401$ AND $R_s = 0.0309$.

j	$R_{\text{out}} =$	$R_{\text{out}} =$	$\rho_j^{(1)}$
	0.4143	0.3955	
	$\lambda_j^{(1)}$	$\lambda_j^{(1)}$	
2	0.483	0.461	0
3	0.155	0.153	0.406
4	0.012	0.012	0
5	0.010	0.010	0.070
6	0.009	0.009	0
7	0.009	0.010	0.033
8	0.011	0.012	0
9	0.014	0.017	0
10	0.015	0.018	0
11	0.012	0.014	0.122
12	0.009	0.011	0
13	0.008	0.009	0.103
14	0.007	0.008	0
15 – 19	0.007	0.007	0
20	0.006	0.006	0.133
21 – 23	0.006	0.006	0
24	0.006	0.006	0.133
25 – 52	0.006	0.006	0
53 – 55	0.007	0.007	0

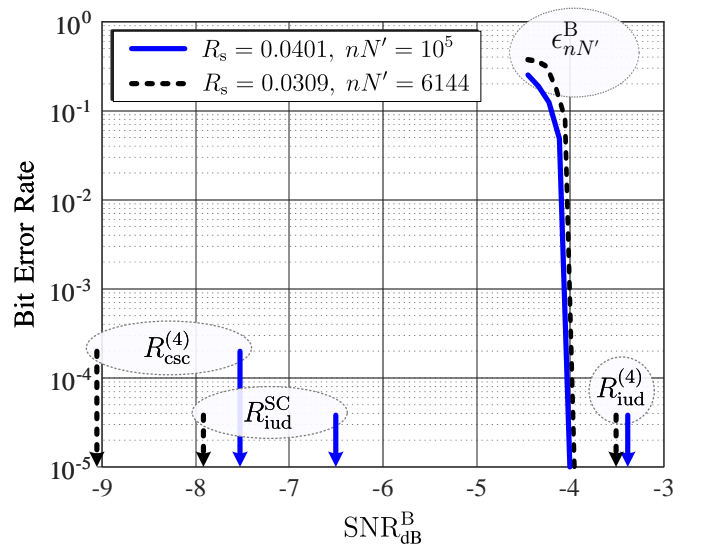


Fig. 14: The bit error rate of the constructed code $\epsilon_{nN'}^B$, the i.u.d. secure rate $R_{\text{iud}}^{(4)}$, the constrained secrecy capacity $R_{\text{csc}}^{(4)}$ of the 4-th order E-FSMC modeling the ISI-WTC in Example 1, and the i.u.d. secure rate of the superchannel $R_{\text{iud}}^{\text{SC}}$ in Table V at $\text{SNR}_{\text{dB}}^E = -4.0$.

replicate the spectral characteristics of sequences generated by the optimized Markov source, concentrating approximately 88% of the available power in frequency ranges that favor Bob's channel over Eve's, in terms of the gain-to-noise ratio.

B. Performance

We first evaluate the performance of the proposed code for BPSK-modulated codewords of length $nN' = 10^5$. At a secure rate of $R_s = 0.0401$ ($q = 0.1382$), the outer LDPC code is constructed with a punctured blocklength of

$N' = 25000$ using the optimized degree distributions from Table III ($R_{\text{out}} = 0.4143$, $R'_{\text{out}} = 0.4808$). Combined with a trellis code of rate $R_{\text{in}} = 1/4$ (Table V), this setup results in an overall design rate of $R_{\text{d}} = 0.1202$. Regarding secrecy efficiency, the rate of information leakage is upper bounded by $\varepsilon_{nN'} < 10^{-5}$, as per (17) in Lemma 1, $\lim_{N \rightarrow \infty} \frac{1}{nN} I(\mathbf{D}^{mN}; \mathbf{Z}^{nN}) = 0.080$ (bits/channel use), $\varepsilon_{nN'}^{\text{F}} < 10^{-5}$, and $R_{\text{r}} = 0.0801$. Regarding the reliability efficiency, the proposed code achieves a bit-error rate (BER) $\varepsilon_{nN'}^{\text{B}} < 10^{-5}$ for $\text{SNR}_{\text{dB}}^{\text{B}} = -4$ at Bob's decoder. In addition, for a blocklength of $nN' = 6144$, the proposed code demonstrates almost the same reliability and secrecy performance at a secure rate of $R_{\text{s}} = 0.0309$ ($q = 0.1100$) using the optimized degree distributions of Table III ($R_{\text{out}} = 0.3955$, $R'_{\text{out}} = 0.4444$) and a trellis code of rate $R_{\text{in}} = 1/4$ in Table V.

The BER simulation curve is shown in Fig. 14. For comparison, this figure also includes the i.u.d. secure rate $R_{\text{iud}}^{(4)}$, the constrained secrecy capacity $R_{\text{csc}}^{(4)}$ of the fourth-order E-FSMC modeling the ISI-WTC in Example 1, and the i.u.d. secure rate of the superchannel $R_{\text{iud}}^{\text{SC}}$ in Table V, all evaluated at $\text{SNR}_{\text{dB}}^{\text{E}} = -4.0$. As illustrated, the designed concatenated code achieves a reliability threshold that is 2.5 dB away from $R_{\text{iud}}^{\text{SC}}$, 3.6 dB away from $R_{\text{csc}}^{(4)}$, and surpasses $R_{\text{iud}}^{(4)}$ by 0.6 dB for a blocklength of $nN' = 10^5$. In addition, the code simulation shows that, for $nN' = 6144$, a BER of 10^{-5} is achieved at an SNR that surpasses $R_{\text{iud}}^{(4)}$ by 0.4 dB.

VII. CONCLUSION

In this paper, we have proposed a two-stage concatenated code over ISI-WTCs. We have incorporated a trellis code at the inner stage and defined the concept of a superchannel as a joint model for trellis codes at the input of the ISI-WTCs. We have designed the inner-stage trellis code so that it transforms the i.u.d. input process into a Markov output process that achieves the constrained secrecy capacity. Accordingly, the i.u.d. secure rate of the resulting superchannel asymptotically approaches the constrained secrecy capacity of the constituent ISI-WTC, enabling the two-stage code to exceed the i.u.d. secure rate of the ISI-WTC. Numerical results show that, even in finite blocklength regimes, the proposed two-stage code can leverage spectral differences between Bob's and Eve's channels to achieve positive secure rates despite Eve's channel having a higher point-to-point unconstrained capacity than Bob's.

VIII. ACKNOWLEDGMENT

The authors are grateful to Prof. Pascal O. Vontobel for helpful discussions and invaluable comments on the earlier versions of this manuscript.

APPENDIX A SIMULATION SCENARIO

In phased arrays, the deviation between the reference beam angle and the steering beam angle introduces a finite time delay between the signals due to the different propagation paths originating from or arriving at various antenna elements. This results in signal overlap and interference when the signals are

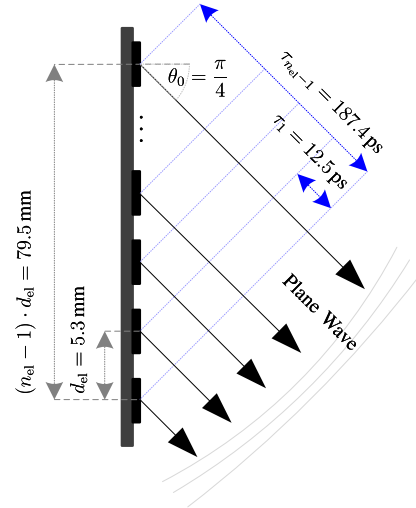


Fig. 15: Time delays between transmitted signals from the antenna elements of a 16×16 phased array in the azimuth plane.

combined using a Wilkinson combiner. Let $\lambda_c \in \mathbb{R}$ represent the wavelength of the carrier signal. We consider a phased array, as described in [12], consisting of a 16×16 antenna grid with elements spaced $d_{\text{el}} \approx 0.5\lambda_c$ apart. Our model is based on an azimuth-plane scan angle of $-\pi/3 \leq \theta_0 \leq \pi/3$ with $n_{\text{el}} = 16$ channels to simulate the varying delays imposed by columns in the array (Fig. 15). For $0 \leq r \leq n_{\text{el}} - 1$, let $\tau_r \in \mathbb{R}$ ($\tau_0 \leq \tau_1 \leq \dots \leq \tau_{n_{\text{el}}-1}$) denote the time delay of the signal from the r -th antenna element in the azimuth plane. Obviously, we have

$$\tau_r = \frac{r \cdot d_{\text{el}} \cdot \sin(\theta_0)}{c}, \quad (\text{for all } 0 \leq r \leq n_{\text{el}} - 1) \quad (23)$$

where d_{el} (≈ 5.3 mm [12]) is the spacing between antenna elements and c is the speed of light.

A. Estimating the Downlink Channel

Let $X(t_c), Y(t_c), N(t_c) \in \mathbb{C}$ (with $t_c \in \mathbb{R}$) denote continuous-time random signals¹⁶ corresponding to the channel's input, the channel's output, and an additive noise, respectively. When local oscillators at the transmitter and the receiver terminals are synchronized, the received signal is expressed as

$$Y(t_c) \triangleq \sum_{r=0}^{n_{\text{el}}-1} |g_{\text{el}}| e^{i \frac{-2\pi c}{\lambda_c} \tau_r} \cdot X(t_c - \tau_r) + N(t_c),$$

where i represents the imaginary unit and $|g_{\text{el}}|$ denotes the element gain of the phased array. Fig. 16 illustrates a typical power-delay profile of a multipath channel, resulting from the considered phased array when used with a normalized element gain $|g_{\text{el}}| = 1$, a carrier frequency of 28 GHz ($\lambda_c = 10.71$ mm), and a steering beam angle of $\theta_0 = \pi/4$, leading to $\tau_r = r \cdot 12.5$ ps and $\tau_{n_{\text{el}}-1} = 187.4$ ps according to (23).

The continuous-time signal $Y(t_c)$ is sampled at the receiver with a symbol interval $T \in \mathbb{R}$ and represented by $Y(t) \triangleq Y(t_c)$.

¹⁶The variable $t_c \in \mathbb{R}$ represents continuous time, distinguishing it from the discrete-time variable $t \in \mathbb{Z}$ used throughout the paper. With a slight abuse of notation, we consider a signal to be continuous-time when its argument is continuous ($\in \mathbb{R}$) and discrete-time when its argument is discrete ($\in \mathbb{Z}$).

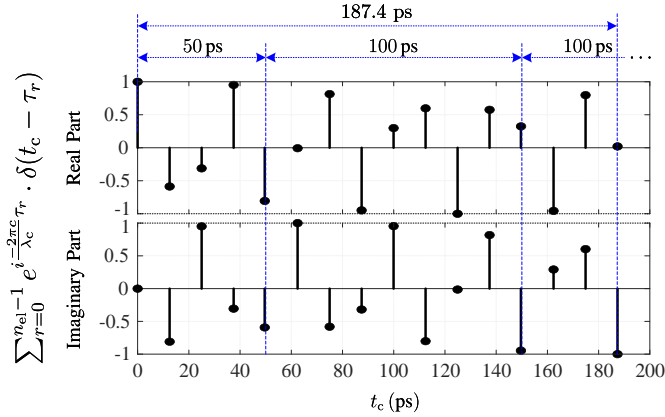


Fig. 16: Power-delay profile of the multipath channel associated with the phased array shown in Fig. 15, when used with a carrier frequency of $c/\lambda_c = 28$ GHz.

TABLE IV: UNNORMALIZED ISI CHANNEL MODEL CORRESPONDING TO THE POWER-DELAY PROFILE SHOWN IN FIG. 16, WITH A SYMBOL INTERVAL OF $T = 100$ ps.

r	Period (ps)	Unnormalized g_r
0	0 – 50	0.2482 – 0.7569 <i>i</i>
1	50 – 150	0.6554 + 0.1116 <i>i</i>
2	150 – 250	–0.1383 – 0.1046 <i>i</i>

T) for $t \in \mathbb{Z}$. In phased arrays, the interference among delayed signals is mitigated using linear multitap equalizers [12]. Nevertheless, this approach is effective only if $T^{-1} \cdot \tau_{n_{\text{el}}-1} < \eta$, where $0 < \eta < 1$ is the equalizer's operating threshold, which is inversely proportional to the noise level.¹⁷ Exceeding the ultimate bound $T^{-1} \cdot \tau_{n_{\text{el}}-1} < 1$ results in noise amplification and residual ISI in multitap equalizers [62, Ch. 9], [63, Ch. 13], [64, Ch. 8]. Due to (23), this upper bound imposes the constraint $(n_{\text{el}}-1) \cdot d_{\text{el}} \cdot \sin(\theta_0) \cdot T^{-1} < \eta \cdot c$, limiting the number of array elements (n_{el}), the size of the phased array ($\propto d_{\text{el}}$), the range of the supported scan angles (θ_0), and the symbol rate of the communication system (T^{-1}).

To verify the efficiency of our proposed coding scheme, we consider BPSK waveforms with a symbol rate of 10 Gbaud ($T = 100$ ps and $T^{-1} \cdot \tau_{n_{\text{el}}-1} = 1.874$) under a high level of Gaussian noise ($\text{SNR}_{\text{dB}} = -4.0$). As shown in Fig. 16, the unnormalized ISI tap coefficients are captured by sampling at $\frac{T}{2} + t \cdot T$ for $t \in \{1, 2, 3\}$ (see Table IV). Accordingly, the normalized transfer polynomial¹⁸ of the downlink channel from the considered phased array, obtained by sampling the output of a filter matched to the shaping pulse at the receiver, becomes

$$g[D] = (0.2360 - 0.7195i) + (0.6230 + 0.1061i)D + (-0.1314 - 0.0994i)D^2.$$

¹⁷The scaled version of the term η is referred to as the ISI percentage, denoted by $\text{ISI}_{\%} \triangleq 100 \cdot \eta$ in the literature.

¹⁸A normalized transfer polynomial $g(D) \triangleq \sum_{r=0}^m g_r D^r \in \mathbb{C}[D]$ has to satisfy $\sum_{r=0}^m |g_r|^2 = 1$.

B. Eavesdropping Scenario

We consider a setup where Alice employs a phased array (as described in the previous section) to transmit a signal to Bob's receiver, located at an angle of $\theta^{\text{B}} = \pi/4$ relative to the array's broadside (perpendicular to the array plane). The phased array steers its main lobe towards $\theta_0 = \pi/4$ to maximize signal strength at Bob's location. Meanwhile, Eve, positioned at an angle of $\theta^{\text{E}} = \pi/6$, intercepts the transmitted signals either through the side lobes or, if the main lobe is sufficiently broad to cover $\theta^{\text{E}} = \pi/6$, through the main lobe itself. In this scenario, Eve benefits from an advantage in steering beam angle, meaning the signals she receives experience smaller delays between antenna elements. On the other hand, Bob experiences the full strength of the main lobe, typically resulting in a higher SNR. To create a more challenging adversarial scenario, we assume $\text{SNR}_{\text{dB}}^{\text{B}} = \text{SNR}_{\text{dB}}^{\text{E}} = -4.0$, keeping the setting advantageous for Eve. Using the calculations from the previous section, we can easily verify that

$$\begin{aligned} g_{\text{B}}[D] &= (0.2360 - 0.7195i) + (0.6230 + 0.1061i)D \\ &\quad + (-0.1314 - 0.0994i)D^2, \\ g_{\text{E}}[D] &= (0.5211 - 0.4792i) + (-0.5791 + 0.4043i)D, \end{aligned} \quad (24)$$

for this considered setup.

As described in [13], to verify Eve's channel advantage over Bob's channel, we employ the well-known water-pouring formulation to analyze the capacities of the point-to-point channels $(g_{\text{B}}[D], \sigma_{\text{B}}^2)$ and $(g_{\text{E}}[D], \sigma_{\text{E}}^2)$. Let E_s denote the average energy per input symbol, and let $W \triangleq \frac{1}{2T}$ represent the bandwidth of a perfect low-pass filter with sampling at the Nyquist frequency $1/T$ at the receiver. Then, the unconstrained (besides some average-energy constraint) capacity of an ISI channel, described by $(g[D] = \sum_{t=0}^{\nu} g(t) \cdot D^t, \sigma^2)$, is calculated by

$$C(g, W) = \frac{1}{2} \cdot \int_{-\infty}^{\infty} \log^+ \left(\frac{\alpha}{2\sigma^2 |G(f)|^2} \right) df,$$

where

$$G(f) = \begin{cases} \frac{\sum_{t=0}^{\nu} g(t) e^{-i2\pi f t T}}{\sqrt{\sum_{t=0}^{\nu} |g(t)|^2}} & (\text{if } |f| \leq W) \\ 0 & (\text{otherwise}) \end{cases},$$

and where $\alpha > 0$ is chosen such that

$$E_s = \int_{-\infty}^{\infty} \left(\alpha - \frac{2\sigma^2}{|G(f)|^2} \right)^+ df.$$

As illustrated in Fig. 17, for a normalized energy constraint $E_s = 1$ and $\text{SNR}_{\text{dB}}^{\text{B}} = \text{SNR}_{\text{dB}}^{\text{E}} = -4.0$, Eve's channel (25) has a higher unconstrained capacity than Bob's channel (24) for sufficiently large bandwidth, confirming Eve's advantage in channel quality.¹⁹

¹⁹Since the unconstrained capacity given by the water-pouring formulation is achieved by Gaussian inputs, caution should be executed when leveraging insights from the presented results, which are solely used to compare the point-to-point channels in the ISI-WTC setup when used with BPSK inputs.

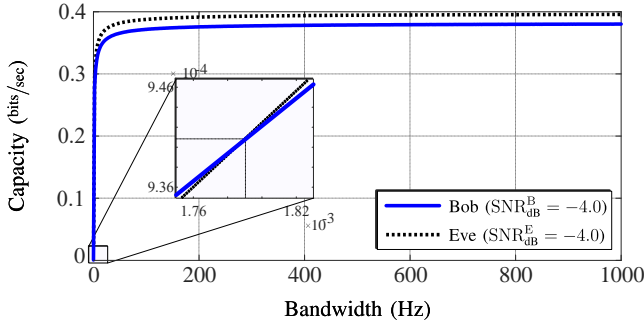


Fig. 17: Unconstrained capacities of Bob’s and Eve’s point-to-point channels in bits/sec with normalized average-energy constraint $E_s = 1$.

APPENDIX B PROOF OF PROPOSITION 1

Note that the proof in this section is only valid for the specific FSMCs and E-FSMCs modeling the ISI-WTCs (i.e., Remarks 1 and 2). We begin by introducing an input setup through which the FSMCs become equivalent to vector input/vector output stationary memoryless wiretap channels, as presented in [45]. This approach leads us to the achievability result and, using the converse part of [45, Thm. 3], establishes the secrecy capacity.

We consider the case in which the input process of the FSMC $\{X(t)\}_{t \in \mathbb{Z}}$ is chosen from a block i.i.d. process $\{X^n(t)\}_{t \in \mathbb{Z}}$. To ensure no interference across the output blocks, for an arbitrary value of $\nu \geq \max\{\nu^B, \nu^E\}$ and all $t \in \mathbb{Z}$, we set $X(nt - \nu + 1) \triangleq 0, \dots, X(nt) \triangleq 0$ while allowing $\{X(n(t-1) + 1) \cdots X(nt - \nu)\}_{t \in \mathbb{Z}}$ to follow an arbitrary but identical distribution over each block. Since ISI-WTCs are represented by *indecomposable* FSMCs, the influence of the initial states $\{S_f(nt)\}_{t \in \mathbb{Z}}$ (fixed at zero above) vanishes over the distribution of each block in $\{S_f^n(t+1)\}_{t \in \mathbb{Z}}$ for a sufficiently large n ($> \nu$), leading to block-wise independence within $\{S_f^n(t)\}_{t \in \mathbb{Z}}$. Moreover, the *stationarity* of the FSMC implies that $S_f^n(t)$ follows an identical stationary distribution for every $t \in \mathbb{Z}$, resulting in a block i.i.d. state process—due to the choice of $\{X^n(t)\}_{t \in \mathbb{Z}}$ and since the FSMC’s states are driven by the input process. Accordingly, since Bob’s channel is assumed to be independent of Eve’s channel, we can write

$$p_{Y^{nN} | X^{nN}, S_f^{nN}}(\mathbf{y}^{nN} | \mathbf{x}^{nN}, \mathbf{s}_f^{nN}) = \prod_{t=1}^N p_{Y^n(t) | X^n(t), S_f^n(t)}(\mathbf{y}^n(t) | \mathbf{x}^n(t), \mathbf{s}_f^n(t)), \quad (26)$$

$$p_{Z^{nN} | X^{nN}, S_f^{nN}}(\mathbf{z}^{nN} | \mathbf{x}^{nN}, \mathbf{s}_f^{nN}) = \prod_{t=1}^N p_{Z^n(t) | X^n(t), S_f^n(t)}(\mathbf{z}^n(t) | \mathbf{x}^n(t), \mathbf{s}_f^n(t)), \quad (27)$$

where the factors on the RHS are independent of t . Note that the factorizations in (26) and (27) are equivalent to the definition of a stationary memoryless wiretap channel in [45] when used with the input process $\{X^n(t)\}_{t \in \mathbb{Z}}$, the output processes $\{Y^n(t)\}_{t \in \mathbb{Z}}$ and $\{Z^n(t)\}_{t \in \mathbb{Z}}$, and the state process $\{S_f^n(t)\}_{t \in \mathbb{Z}}$. Furthermore, the alphabets corresponding to the channel’s input, Bob’s observation, Eve’s observation, and the

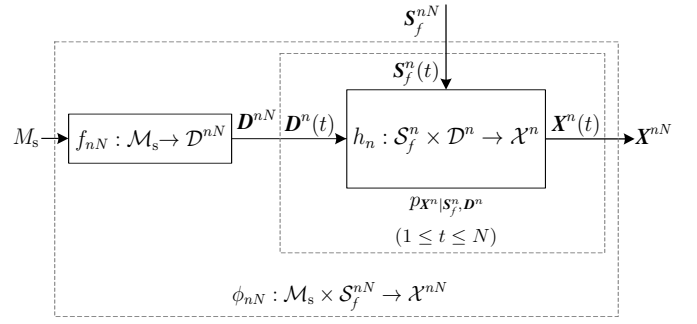


Fig. 18: Generalization of the one-time stochastic encoder in [45].

FSMC’s state are, respectively, set to be $\mathcal{X}^n, \mathcal{Y}^n, \mathcal{Z}^n$, and S_f^n for the equivalent stationary memoryless wiretap channel.

Let $D(t) \in \mathcal{D}$ be an auxiliary random variable such that $D^n(t) \perp S_f^n(t)$ for all $t \in \mathbb{Z}$, complying with Markov chains

$$D^n(t) \rightarrow (X^n(t), S_f^n(t)) \rightarrow Y^n(t), \quad (\forall t \in \mathbb{Z}), \quad (28)$$

$$D^n(t) \rightarrow (X^n(t), S_f^n(t)) \rightarrow Z^n(t), \quad (\forall t \in \mathbb{Z}). \quad (29)$$

According to (28) and (29), we define the following auxiliary channel at the input of the FSMC

$$p_{X^{nN} | S_f^{nN}, D^{nN}}(\mathbf{x}^{nN} | \mathbf{s}_f^{nN}, \mathbf{d}^{nN}) = \prod_{t=1}^N p_{X^n(t) | S_f^n(t), D^n(t)}(\mathbf{x}^n(t) | \mathbf{s}_f^n(t), \mathbf{d}^n(t)). \quad (30)$$

The encoder for the capacity-achieving code—defined as a generalized version of the one-time stochastic encoder presented in [45]²⁰—consists of the concatenation of a nested code’s encoder for wiretap channels $f_{nN} : \mathcal{M}_s \rightarrow \mathcal{D}^{nN}$ with a component-wise stochastic encoder $h_n : S_f^n \times \mathcal{D}^n \rightarrow \mathcal{X}^n$ operating based on the stochastic map in (30), resulting in $\phi_{nN} : \mathcal{M}_s \times S_f^{nN} \rightarrow \mathcal{X}^{nN}$ (see Fig. 18). Specifically, we have $\phi_{nN}(m_s, \mathbf{s}_f^{nN}) \triangleq \left(h_n(\mathbf{s}_f^n(t), \mathbf{d}^n(t)) \right)_{t=1}^N$, where $\mathbf{d}^{nN} \triangleq f_{nN}(m_s)$. Due to [45, Thm. 3], by using this coding scheme, all secure rates R_s satisfying $R_s < \frac{1}{n}(I(\mathbf{D}^n; \mathbf{Y}^n) - I(\mathbf{D}^n; \mathbf{Z}^n))$ are achievable, which corresponds to the achievability region for the equivalent vector input/vector output stationary memoryless wiretap channel described by (26) and (27).²¹

According to the converse part of [45, Thm. 3], it is straightforward to verify that all achievable secure rates R_s , satisfying the reliability criterion in (4) and the strong secrecy criterion $N \cdot \varepsilon_N \rightarrow 0$ (as $N \rightarrow \infty$), are upper-bounded by $R_s \leq \frac{1}{n} \sup_{p_{D^n} : D^n \perp S_f^n} (I(\mathbf{D}^n; \mathbf{Y}^n) - I(\mathbf{D}^n; \mathbf{Z}^n))$. The equivalence between $S_f^n(t)$ and $S_e(t)$, for all $t \in \mathbb{Z}$, concludes the proof.

²⁰The assumption of available one-time state information accurately models our setup for FSMCs representing ISI-WTCs. Specifically, since the FSMC’s states are driven by the inputs and the transfer polynomials $g_B[D]$ and $g_E[D]$ are assumed to be available at Alice’s encoder, the previous state and the current channel input enable her to determine the current state of the FSMC.

²¹The secrecy criterion employed in [45] is stronger than the strong secrecy criterion $N \cdot \varepsilon_N \rightarrow 0$ (as $N \rightarrow \infty$). Therefore, the achievability results are also valid under the strong secrecy and weak secrecy criteria specified by (4).

REFERENCES

- [1] A. Nouri and R. Asvadi, "Matched information rate codes for binary-input intersymbol interference wiretap channels," in *Proc. IEEE Int. Symp. Inf. Theory*, Espoo, Finland, June 2022, pp. 1163–1168.
- [2] C. Gidney and M. Ekerå, "How to factor 2048 bit RSA integers in 8 hours using 20 million noisy qubits," *Quantum*, vol. 5, p. 433, Apr. 2021.
- [3] S. Pirandola, U. L. Andersen, L. Banchi, M. Berta, D. Bunandar, R. Colbeck, D. Englund, T. Gehring, C. Lupo, C. Ottaviani, J. L. Pereira, M. Razavi, J. S. Shaari, M. Tomamichel, V. C. Usenko, G. Vallone, P. Villaresi, and P. Wallden, "Advances in quantum cryptography," *Adv. Opt. Photon.*, vol. 12, no. 4, pp. 1012–1236, Dec. 2020.
- [4] A. D. Wyner, D. Elkouss, and R. Hanson, "Quantum internet: A vision for the road ahead," *Science*, vol. 362, no. 6412, Oct. 2018.
- [5] A. S. Cacciapuoti, M. Caleffi, R. Van Meter, and L. Hanzo, "When entanglement meets classical communications: Quantum teleportation for the quantum internet," *IEEE Trans. Commun.*, vol. 68, no. 6, pp. 3808–3833, June 2020.
- [6] D. Mayers, "Unconditionally secure quantum bit commitment is impossible," *Phys. Rev. Lett.*, vol. 78, pp. 3414–3417, Apr. 1997.
- [7] A. D. Wyner, "The wire-tap channel," *Bell Syst. Tech. J.*, vol. 54, no. 8, pp. 1355–1387, Oct. 1975.
- [8] M. Bloch, O. Günlü, A. Yener, F. Oggier, H. V. Poor, L. Sankar, and R. F. Schaefer, "An overview of information-theoretic security and privacy: Metrics, limits and applications," *IEEE J. Sel. Areas Inf. Theory*, vol. 2, no. 1, pp. 5–22, Mar. 2021.
- [9] M. Mitev, T. M. Pham, A. Chorti, A. N. Barreto, and G. Fettweis, "Physical layer security—from theory to practice," *IEEE BITS Inf. Theory Mag.*, vol. 3, no. 2, pp. 67–79, Dec. 2023.
- [10] J. Choi, "Single-carrier index modulation for IoT uplink," *IEEE J. Sel. Top. Signal Process.*, vol. 13, no. 6, pp. 1237–1248, Oct. 2019.
- [11] M. Sahin and H. Arslan, "Inter-symbol interference in high data rate UWB communications using energy detector receivers," in *Proc. IEEE Int. Conf. on Ultra-Wideband*, Zurich, Switzerland, Sept. 2005, pp. 176–179.
- [12] Z. Zhang, Y. Yin, and G. M. Rebeiz, "Intersymbol interference and equalization for large 5G phased arrays with wide scan angles," *IEEE Trans. Microw. Theory Techn.*, vol. 69, no. 3, pp. 1955–1964, Mar. 2021.
- [13] A. Nouri, R. Asvadi, J. Chen, and P. O. Vontobel, "Constrained secrecy capacity of finite-input intersymbol interference wiretap channels," *IEEE Trans. Commun.*, vol. 71, no. 6, pp. 3301–3316, June 2023.
- [14] G. Forney, "Maximum-likelihood sequence estimation of digital sequences in the presence of intersymbol interference," *IEEE Trans. Inf. Theory*, vol. 18, no. 3, pp. 363–378, May 1972.
- [15] Y. Li, B. Vucetic, and Y. Sato, "Optimum soft-output detection for channels with intersymbol interference," *IEEE Trans. Inf. Theory*, vol. 41, no. 3, pp. 704–713, May 1995.
- [16] C. Douillard, M. Jézéquel, C. Berrou, D. Electronique, A. Picart, P. Didier, and A. Glavieux, "Iterative correction of intersymbol interference: turbo-equalization," *Eur. Trans. Telecommun.*, vol. 6, no. 5, pp. 507–511, Sept. 1995.
- [17] T. V. Souvignier, M. Oberg, P. H. Siegel, R. E. Swanson, and J. K. Wolf, "Turbo decoding for partial response channels," *IEEE Trans. Commun.*, vol. 48, no. 8, pp. 1297–1308, Aug. 2000.
- [18] M. Oberg and P. H. Siegel, "Performance analysis of turbo-equalized partial response channels," *IEEE Trans. Commun.*, vol. 49, no. 3, pp. 436–444, Mar. 2001.
- [19] B. M. Kurkoski, P. H. Siegel, and J. K. Wolf, "Joint message-passing decoding of LDPC codes and partial-response channels," *IEEE Trans. Inf. Theory*, vol. 48, no. 6, pp. 1410–1422, June 2002.
- [20] A. Kavčić, X. Ma, and M. Mitzenmacher, "Binary intersymbol interference channels: Gallager codes, density evolution, and code performance bounds," *IEEE Trans. Inf. Theory*, vol. 49, no. 7, pp. 1636–1652, July 2003.
- [21] G. Colavolpe and G. Germei, "On the application of factor graphs and the sum-product algorithm to ISI channels," *IEEE Trans. Commun.*, vol. 53, no. 5, pp. 818–825, May 2005.
- [22] A. Anastasopoulos, K. M. Chugg, G. Colavolpe, G. Ferrari, and R. Raheli, "Iterative detection for channels with memory," *Proc. IEEE*, vol. 95, no. 6, pp. 1272–1294, June 2007.
- [23] S. Zheng, Y. Liu, and P. H. Siegel, "PR-NN: RNN-based detection for coded partial-response channels," *IEEE J. Sel. Areas Commun.*, vol. 39, no. 7, pp. 1967–1982, July 2021.
- [24] C. Berrou, A. Glavieux, and P. Thitimajshima, "Near shannon limit error-correcting coding and decoding: Turbo-codes. 1," in *Proc. IEEE Int. Conf. Commun.*, vol. 2, 1993, pp. 1064–1070 vol.2.
- [25] L. E. Baum and T. Petrie, "Statistical inference for probabilistic functions of finite state Markov chains," *Ann. Math. Stat.*, vol. 37, no. 6, pp. 1554–1563, Dec. 1966.
- [26] P. L. McAdam, L. R. Welch, and C. L. Weber, "M.A.P. bit decoding of convolutional codes," in *Proc. IEEE Int. Symp. Information Theory*, Asilomar, CA, USA, Dec. 1972, p. 91.
- [27] L. Bahl, J. Cocke, F. Jelinek, and J. Raviv, "Optimal decoding of linear codes for minimizing symbol error rate," *IEEE Trans. Inf. Theory*, vol. 20, no. 2, pp. 284–287, Mar. 1974.
- [28] T. J. Richardson, M. A. Shokrollahi, and R. L. Urbanke, "Design of capacity-approaching irregular low-density parity-check codes," *IEEE Trans. Inf. Theory*, vol. 47, no. 2, pp. 619–637, Feb. 2001.
- [29] N. Varnica and A. Kavčić, "Optimized low-density parity-check codes for partial response channels," *IEEE Commun. Lett.*, vol. 7, no. 4, pp. 168–170, Apr. 2003.
- [30] X. Jiao, J. Mu, Y. C. He, and W. Xu, "Linear-complexity ADMM updates for decoding LDPC codes in partial response channels," *IEEE Commun. Lett.*, vol. 23, no. 12, pp. 2200–2204, Dec. 2019.
- [31] X. Jiao, H. Liu, J. Mu, and Y. C. He, " l_2 -box ADMM decoding for LDPC codes over ISI channels," *IEEE Trans. Veh. Technol.*, vol. 70, no. 4, pp. 3966–3971, Apr. 2021.
- [32] T. Wadayama, "Interior point decoding for linear vector channels based on convex optimization," *IEEE Trans. Inf. Theory*, vol. 56, no. 10, pp. 4905–4921, Oct. 2010.
- [33] S. Boyd, N. Parikh, E. Chu, B. Peleato, and J. Eckstein, "Distributed optimization and statistical learning via the alternating direction method of multipliers," *Found. Trends Mach. Learn.*, vol. 3, no. 1, pp. 1–122, Jan. 2011.
- [34] J. B. Soriaga, H. D. Pfister, and P. H. Siegel, "Determining and approaching achievable rates of binary intersymbol interference channels using multistage decoding," *IEEE Trans. Inf. Theory*, vol. 53, no. 4, pp. 1416–1429, Apr. 2007.
- [35] A. Kavčić, X. Ma, and N. Varnica, "Matched information rate codes for partial response channels," *IEEE Trans. Inf. Theory*, vol. 51, no. 3, pp. 973–989, Mar. 2005.
- [36] S. Leung-Yan-Cheong and M. Hellman, "The Gaussian wire-tap channel," *IEEE Trans. Inf. Theory*, vol. 24, no. 4, pp. 451–456, July 1978.
- [37] M. Baldi, M. Bianchi, and F. Chiaraluce, "Non-systematic codes for physical layer security," in *Proc. IEEE Inf. Theory Workshop*, Dublin, Ireland, Sept. 2010, pp. 1–5.
- [38] D. Klinc, J. Ha, S. W. McLaughlin, J. Barros, and B. J. Kwak, "LDPC codes for the Gaussian wiretap channel," *IEEE Trans. Inf. Forensics Secur.*, vol. 6, no. 3, pp. 532–540, Sept. 2011.
- [39] C. W. Wong, T. F. Wong, and J. M. Shea, "LDPC code design for the BPSK-constrained Gaussian wiretap channel," in *Proc. IEEE Glob. Commun. Conf.*, San Antonio, TX, USA, Dec. 2011, pp. 898–902.
- [40] M. Baldi, M. Bianchi, and F. Chiaraluce, "Coding with scrambling, concatenation, and HARQ for the AWGN wire-tap channel: A security gap analysis," *IEEE Trans. Inf. Forensics Secur.*, vol. 7, no. 3, pp. 883–894, June 2012.
- [41] M. Baldi, G. Ricciutelli, N. Maturo, and F. Chiaraluce, "Performance assessment and design of finite length LDPC codes for the Gaussian wiretap channel," in *Proc. IEEE Int. Conf. Commun.*, London, UK, June 2015, pp. 435–440.
- [42] A. Nooraiepour, S. R. Aghdam, and T. M. Duman, "On secure communications over Gaussian wiretap channels via finite-length codes," *IEEE Commun. Lett.*, vol. 24, no. 9, pp. 1904–1908, Sept. 2020.
- [43] B. Dai, Z. Ma, and Y. Luo, "Finite state Markov wiretap channel with delayed feedback," *IEEE Trans. Inf. Forensics Secur.*, vol. 12, no. 3, pp. 746–760, Mar. 2017.
- [44] J. de Dieu Mutangana and R. Tandon, "Blind MIMO cooperative jamming: secrecy via ISI heterogeneity without CSIT," *IEEE Trans. Inf. Forensics Secur.*, vol. 15, pp. 447–461, 2020.
- [45] T. S. Han, H. Endo, and M. Sasaki, "Wiretap channels with one-time state information: strong secrecy," *IEEE Trans. Inf. Forensics Secur.*, vol. 13, no. 1, pp. 224–236, Jan. 2018.
- [46] A. Thangaraj, S. Dihidar, A. R. Calderbank, S. W. McLaughlin, and J. M. Merolla, "Applications of LDPC codes to the wiretap channel," *IEEE Trans. Inf. Theory*, vol. 53, no. 8, pp. 2933–2945, Aug. 2007.
- [47] C. B. Schlegel and L. C. Perez, *Trellis and Turbo Coding: Iterative and Graph-Based Error Control Coding, 2nd Edition*. Hoboken, NJ, USA: John Wiley & Sons, 2015.
- [48] J. Wolf and G. Ungerboeck, "Trellis coding for partial-response channels," *IEEE Trans. Commun.*, vol. 34, no. 8, pp. 765–773, Aug. 1986.
- [49] G. Forney, "Codes on graphs: normal realizations," *IEEE Trans. Inf. Theory*, vol. 47, no. 2, pp. 520–548, Feb. 2001.

- [50] P. O. Vontobel, A. Kavčić, D. M. Arnold, and H. A. Loeliger, "A generalization of the Blahut-Arimoto algorithm to finite-state channels," *IEEE Trans. Inf. Theory*, vol. 54, no. 5, pp. 1887–1918, May 2008.
- [51] R. G. Gallager, *Information Theory and Reliable Communication*. New York, NY, USA: John Wiley & Sons, 1968.
- [52] T. Richardson and R. Urbanke, "Efficient encoding of low-density parity-check codes," *IEEE Trans. Inf. Theory*, vol. 47, no. 2, pp. 638–656, Feb. 2001.
- [53] D. M. Arnold, H. A. Loeliger, P. O. Vontobel, A. Kavčić, and W. Zeng, "Simulation-based computation of information rates for channels with memory," *IEEE Trans. Inf. Theory*, vol. 52, no. 8, pp. 3498–3508, Aug. 2006.
- [54] S. Benedetto, D. Divsalar, G. Montorsi, and F. Pollara, "Algorithm for continuous decoding of turbo codes," *Electron. Lett.*, vol. 32, no. 4, pp. 314–315, Feb. 1996.
- [55] T. J. Richardson and R. L. Urbanke, "The capacity of low-density parity-check codes under message-passing decoding," *IEEE Trans. Inf. Theory*, vol. 47, no. 2, pp. 599–618, Feb. 2001.
- [56] S. Y. Chung, G. D. Forney, T. J. Richardson, and R. Urbanke, "On the design of low-density parity-check codes within 0.0045 dB of the Shannon limit," *IEEE Commun. Lett.*, vol. 5, no. 2, pp. 58–60, Feb. 2001.
- [57] T. Richardson and R. Urbanke, "Thresholds for turbo codes," in *Proc. IEEE Int. Symp. Inf. Theory*, Sorrento, Italy, June 2000.
- [58] H. Pfister, J. Soriaga, and P. Siegel, "On the achievable information rates of finite state ISI channels," in *Proc. IEEE Glob. Commun. Conf.*, San Antonio, TX, USA, Nov. 2001, pp. 2992–2996.
- [59] Y. C. Ho, "An explanation of ordinal optimization: Soft computing for hard problems," *Inf. Sci.*, vol. 113, no. 3, pp. 169–192, Mar. 1999.
- [60] H. Imai and S. Hirakawa, "A new multilevel coding method using error-correcting codes," *IEEE Trans. Inf. Theory*, vol. 23, no. 3, pp. 371–377, May 1977.
- [61] 3rd Generation Partnership Project (3GPP), "3GPP TS 38.212: multiplexing and channel coding for 5G NR (release 15)," 3GPP, Technical Specification 38.212, 2018.
- [62] J. G. Proakis, *Digital Communications*, 4th ed. New York, NY, USA: McGraw-Hill Education, 2001.
- [63] S. Haykin, *Adaptive Filter Theory*, 3rd ed. Upper Saddle River, NJ, USA: Prentice Hall, 1996.
- [64] A. Goldsmith, *Wireless Communications*. Cambridge, UK: Cambridge University Press, 2005.